Applied Catalysis B: Environmental 170-171 (2015) 90–123

Contents lists available at ScienceDirect

Applied Catalysis B: Environmental

journal homepage: www.elsevier.com/locate/apcatb

Review

Solar photocatalysis: Materials, reactors, some commercial, and pre-industrialized applications. A comprehensive approach

Danilo Spasiano[a], Raffaele Marotta[a,*], Sixto Malato[b], Pilar Fernandez-Ibañez[b], Ilaria Di Somma[c]

[a] Dipartimento di Ingegneria Chimica, dei Materiali e della Produzione Industriale, Università degli Studi di Napoli "Federico II", P.le V. Tecchio, 80, 80125, Napoli, Italy
[b] Plataforma Solar de Almería-CIEMAT, Carretera de Senés Km 4, 04200, Tabernas, Almería, Spain
[c] Istituto di Ricerche sulla Combustione, Consiglio Nazionale delle Ricerche (CNR), P.le V. Tecchio, 80, 80125, Napoli, Italy

ARTICLE INFO

Article history:
Received 14 October 2014
Received in revised form
22 December 2014
Accepted 31 December 2014
Available online 7 January 2015

Keywords:
Solar photocatalysis
Solar photoreactors
Solar chemical production
Solar photocatalytic technology
Green photochemistry

ABSTRACT

In the future, solar energy, along with other renewable resources, could play a key role in mass production of fine chemicals. It could also potentially solve environmental problems, as demonstrated by recent developments in the use of solar energy, such as solar photocatalysis. The solar photocatalytic technology has been demonstrated to be effective for:

- Treating groundwater, drinking water, industrial wastewater, and air and soil pollution,
- Water disinfection, and
- Industrial production of fine chemicals.

This report summarizes the current status of solar photocatalysis and identifies future opportunities for research and industry in this field, including recent relevant bibliography. The main commercial solar photocatalytic applications are described, included the technologies based on sunlight for antifogging and self-cleaning of coating materials, glass, and concrete. An overview of several different solar photoreactors and the main operating process parameters are also provided. For the estimation of capital costs, it is suggested the use of appropriate "figures of merit". The present review would be of interest for researchers, technologists, engineers, and industrialists.

Contents

* Corresponding author. Tel.: +39 81 7682968; fax: +39 81 5936936.
E-mail address: raffaele.marotta@unina.it (R. Marotta).

http://dx.doi.org/10.1016/j.apcatb.2014.12.050
0926-3373/

1. Introduction

Since non-renewable energy resources are being depleted [1], alternative sources, such as solar, wind, and geothermal energies, will acquire an increasingly important role in the near future. This is particularly true of solar energy, which may be converted into chemical energy by natural solar photo-assisted reactions.

Among the solar photoreactions, photocatalysis is the most widely studied, and is applied on different levels and in such different industries as fine chemical production, architecture and construction, water and air treatment, hygiene and sanitation, environmental protection, and the automotive industry [2–8].

Photocatalytic products were first marketed in Japan in the mid-1990s, and later in America and Europe. By 2009, the global volume of solar photocatalysis-based products was $848 million and is expected to double in 2014, reaching nearly $1.7 billion [9] (Fig. 1).

In 2009, photocatalytic products for construction accounted for the largest share of the market (over 87%), with estimated gains of $740.3 million. At a predicted compound annual growth rate (CAGR) of 14.5%, these will reach $1.5 billion in 2014 [10]. The consumer products market segment was worth $85 million for the same year, and is expected to grow at a CAGR of 13.2% to $158 million in 2014.

Other products contributed with smaller sales volumes totaling $22.1 million. The market is projected to reach $33.6 million in 2014 at a 5-year CAGR of 8.7%. However, extensive research continues to further improve the photocatalytic technology and extend its potential uses, revealing that in the future they may provide realistic solutions to most major modern dilemmas: depletion of stocks of fossil fuels, progressive pollution of natural resources, and global warming. Some improvements in the performance of solar photocatalytic applications have also been related to advances in nanotechnology. In particular, the synthesis and manufacture of new photocatalysts, using nanotechnologies, show that it is possible to greatly enhance the photocatalytic efficiency of specific materials [11,12].

1.1. Historical background

The use of solar energy in chemical synthesis had not been explored until the beginning of the 20th century when Ciamician, called the "Father of Modern Photochemistry" [13], began to study the chemical behavior of organic compounds under solar irradiation. One of the first milestones in the use of solar photochemistry was the technical-scale production of ascaridole (an anthelmintic drug) by Schenck in 1943, by solar irradiation of α-terpinene [14]:

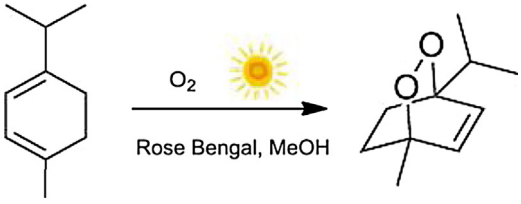

(r1)

The first solar chemical plant, a pilot plant to produce ascaridole, was built after World War II [15]. In the second half of the 20th century, with the development of artificial lamps, photochemistry moved indoors [16]. During the 1970s, after the oil crisis, and influenced by growing awareness of global warming, research on the possibility of using the sunlight as an energy source was intensified. During these years, Fujishima and Honda demonstrated the market potential of heterogeneous photocatalysis [17]. In the wake of revival of interest in solar production, new non-concentrating and concentrating solar pilot reactors were designed and built [18]. Several experiments in solar detoxification of aqueous effluents were undertaken during the 1990s [19–22]. The first experimental solar photocatalytic pilot plant, located in Albuquerque (New Mexico, USA), was designed and built in 1989 [23]. Immediately afterwards, in 1990, a similar facility was designed and built at the Plataforma Solar de Almeria (Almeria, Spain) [24]. Since the beginning of the 21st century, applied research has also focused on the use of natural sunlight for preindustrial fine chemical production.

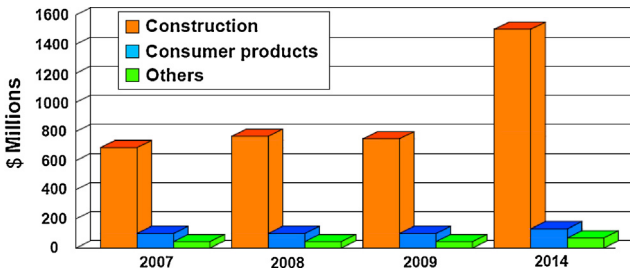

Fig. 1. Global market for photocatalyst products 2007–2014 ($ millions).

1.2. Principles of photocatalytic and sensitized photochemical reactions

The term "photocatalysis" indicates acceleration of a photoreaction due to the presence of a catalyst [25]. This definition also takes into account photosensitization, a chemical process by which one molecular entity is photochemically altered following absorption of radiation by another molecular entity called a photosensitizer. However, unlike a photocatalytic process, photosensitization rules out photoacceleration of a chemical reaction regardless of whether it occurs in a homogeneous or heterogeneous phase.

1.2.1. Homogeneous photocatalysis

The most commonly used homogeneous solar photocatalytic systems at both pilot and commercial scale are photo-Fenton and photo-sensitized oxidation by singlet oxygen. The main photo-Fenton reactions in a solar-assisted catalytic cycle are illustrated in the following simplified scheme [26]:

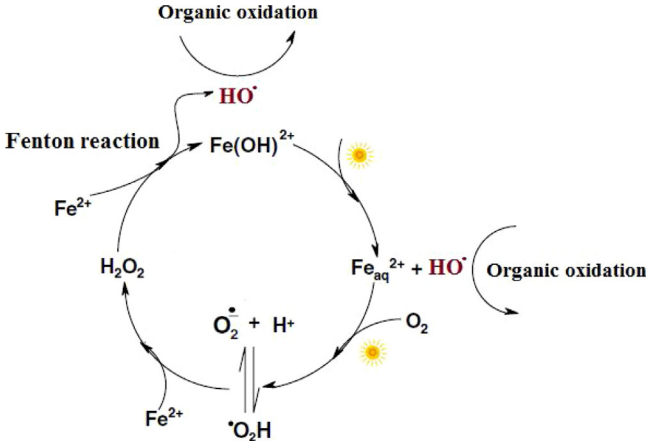

Hydrated ferric ions ($[Fe(OH)]^{2+}$) are photo-reduced to ferrous ions in acidic aqueous solutions in the presence of sunlight radiation with wavelengths shorter than 580 nm, giving rise to hydroxyl radicals ($HO^{\bullet}$). Ferrous ions are reoxidized to ferric by hydrogen peroxide or molecular oxygen, producing additional reactive radicals, like hydroxyl and hydroperoxyl radicals [27,28]. These radicals promptly oxidize organic compounds converting them into carbon dioxide and water [29].

The starting concentrations of hydrogen peroxide and ferrous ions critically influence overall efficiency of the solar oxidation process. Oxidation rates generally increase with iron ions and hydrogen peroxide concentrations [30], even though such increase is sometimes observed to be deleterious at the highest concentrations. In fact, an excess of ferrous ions or hydrogen peroxide can cause inhibition of the solar photochemical oxidation process, because these species may compete with the organic compounds as hydroxyl radical scavengers [31,32]:

$$(r2) \qquad Fe^{2+} + HO^{\bullet} \rightarrow Fe^{3+} + HO^{-}$$

$$(r3) \qquad H_2O_2 + HO^{\bullet} \rightarrow H_2O + HO_2^{\bullet}$$

Photosensitization is a chemical process in which a soluble substance (sensitizer or photosensitizer) is capable of absorbing radiation and transferring the energy absorbed to a different reacting molecule like molecular oxygen (photosensitized oxidation) [33]. In this case, an oxygen molecule in the ground state ($^3O_2$) is excited to a higher energy and an energized species of oxygen, singlet oxygen ($^1O_2$), is formed. This unstable activated species is much more reactive than the ground triplet state and it is responsible for the selective photooxidation of various organic compounds to fine chemicals [34–36]. Since the sensitizer is not usually consumed, or at most, is only partially degraded during the photochemical process, returning to its original state once the reaction is complete, photosensitization may be classified as a photocatalytic reaction [35]. Methylene blue (absorption wavelength max, λ_{max} = 665 nm [37]) and Rose-Bengal (λ_{max} = 550 nm) are the most popular photosensitizers used for the production of singlet oxygen. The homogeneous catalytic or sensitized photooxidation of organic substrates using sunlight as the radiation source is of increasing commercial interest in the fields of production of chemical intermediates and wastewater treatment.

1.2.2. Heterogeneous photocatalysis

A heterogeneous photocatalyst is a semiconducting substance which can be chemically activated by radiation. A band model is often used for schematic representation of the electronic structures of photosemiconducting materials. Many well-documented reviews are devoted to the fundamentals of photocatalysis in this regard [38–44]. If a photosemiconductor is irradiated by light with energy matching or greater than its band gap energy (E_g), an electron (e^-) in an electron-filled valence band (VB) is excited to a vacant conduction band (CB), leaving a positive hole (h^+) in the VB. These photogenerated electrons and positive holes drive reduction and oxidation, respectively, of different compounds, not necessarily adsorbed on the surface of the photocatalyst [45]. Valence band holes (h_{VB}^+) are powerful oxidants, whereas, conduction band electrons (e_{CB}^-) are reductants (Fig. 2). Due to their electronic structures, heterogeneous photocatalysts can act as mediators in chemical redox processes. The first step is the formation of charge carriers by a photon. The excited electrons and holes in the absence of suitable electron and hole scavengers tend to recombine very quickly, dissipating the energy as heat. Photocatalytic activity is strongly dependent on the competition between the surface transfer of charge carriers and electron–hole recombination [46]. If a suitable scavenger or surface defect is available to trap the photogenerated electrons or holes, recombination is limited and further

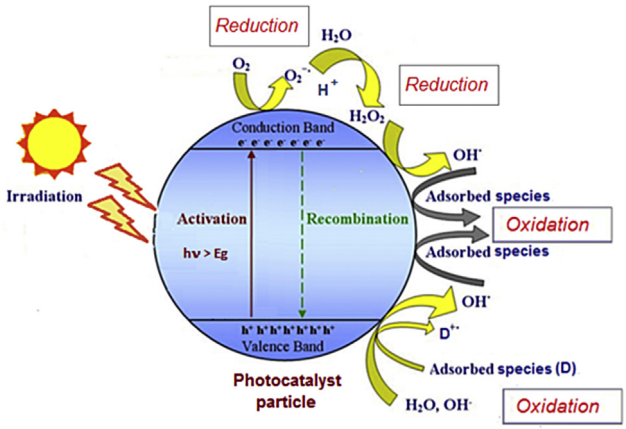

Fig. 2. Schematic illustration of basic mechanism of a solar heterogeneous photocatalytic process.

photocatalytic reactions may occur that yield mineralization products during prolonged reaction periods. The strong oxidizing power of the positive hole can enable a one-electron oxidation step with water, normally present in the system, to produce hydroxyl radicals (HO):

$$(r4) \qquad H_2O + h_{VB}{}^{+} \rightarrow HO^{\bullet} + H^{+}$$

which are highly reactive species able to oxidize organic molecules in liquid or gas phase [38,47]. Moreover, if air is also present, oxygen can act as an electron acceptor, and be reduced by the photoelectrons in the conduction band to form a superoxide ion, which is also a powerful oxidant. The width of the band gap is a measure of the strength of the chemical bond [48]. Semiconductors that are stable under illumination, typically metal oxides, usually consist of the top of the valence band located at +3 eV or lower (vs. NHE). From the standpoint of solar energy, the development of photocatalysts which can drive redox reactions under visible light (>400 nm) is indispensable [49].

Among the photo-semiconductors (ZnO, WO_3, MoO_3, ZrO_2, SnO_2, α-Fe_2O_3, etc.), titanium dioxide (TiO_2, titania) is one of the most promising candidates for commercial solar applications, mainly due to its photochemical stability and high oxidation power (3.2 eV vs. NHE, which corresponds to photons with a wavelength of 388 nm), high resistance to photocorrosion in aqueous environments, safety, and lower cost than other photocatalytic materials [50]. The drawbacks of titania, which currently limit its wider commercial application, are that it absorbs only in the ultraviolet region, which is only about 3–4% of the solar energy reaching the terrestrial surface, and the high rate of electron/hole ($e_{CB}{}^{-}/h_{VB}{}^{+}$) pair recombination. Much effort has been devoted to the development of TiO_2 visible-light harvesting photocatalysts to increase the amount of visible sunlight which TiO_2 can absorb [51].

Most of the research and commercial applications use a heterogeneous photocatalyst, generally titanium dioxide, dispersed in the liquid phase by mechanical agitation or immobilized on a surface, such as the reactor wall, or supported on particles forming a catalytic bed. The use of slurry systems requires a further separation step, such as filtration or centrifugation, which increases the complexity of the overall process and decrease its economic feasibility. However, the suspensions are easier to work with and provide higher efficiencies than immobilized catalysts, mainly due to a higher ratio of active catalytic surface to reaction volume and fewer mass transfer limitations [52].

Moreover, the photocatalyst slurry is easily prepared by several chemical routes [53]. On the contrary, synthesis of immobilized catalysts is more difficult and requires inert support materials, such as alumina pellets, molecular sieves, or glass or ceramic fibers [54].

Commercial titanium dioxide (TiO_2) powders, such as anatase crystalline or anatase and rutile mixtures (Degussa, Evonik, Aeroxide P25, 80:20 anatase/rutile) are the most widely used heterogeneous catalysts for solar wastewater treatment applications, because their detoxification efficiencies are the highest [55].

Two parameters for the characterization of photocatalytic activities in heterogeneous systems, the photonic efficiency and the quantum yield, have been suggested. The photonic efficiency, is generally used to compare the photoactivity of different photocatalysts [56]. This can be derived from analytical data as the ratio of the experimental photocatalytic reaction rate (mol L^{-1} s^{-1}) to the incident photon rate (Einstein L^{-1} s^{-1}) measured by actinometry.

Several different definitions of the second indicator, the quantum yield (Q_y), have been proposed [44,57]. However, these definitions are all based on a ratio involving the number of photoconverted or photoproduced molecules over the number of photons absorbed by the photocatalyst:

$$(eq1) \qquad Q_y = \frac{n^0 \text{ molecules (moles) reacted or produced}}{n^0 \text{ photons (Einsteins) absorbed}}$$

The quantum yield may be estimated by the macroscopic irradiation balance, which takes into account light scattering and photon absorption rates and the net consumption/production of chemicals.

1.2.3. *Photo-induced super-hydrophilicity*

When a thin-film photosemiconductor (e.g., TiO_2) is activated by solar photons, the positive holes diffuse to the surface and react with water molecules adsorbed on it, producing hydroxyl radicals, thus, increasing the number of hydroxyl groups on the TiO_2 surface during irradiation [58]. Consequently, during irradiation, the contact angle between titania surfaces and water molecules gradually closes to near zero. This phenomenon was called photo-induced super-hydrophilicity: if water is added to the irradiated titanium dioxide surface, it does not form spherical droplets as in the dark, and is not repelled, but forms a highly uniform thin film.

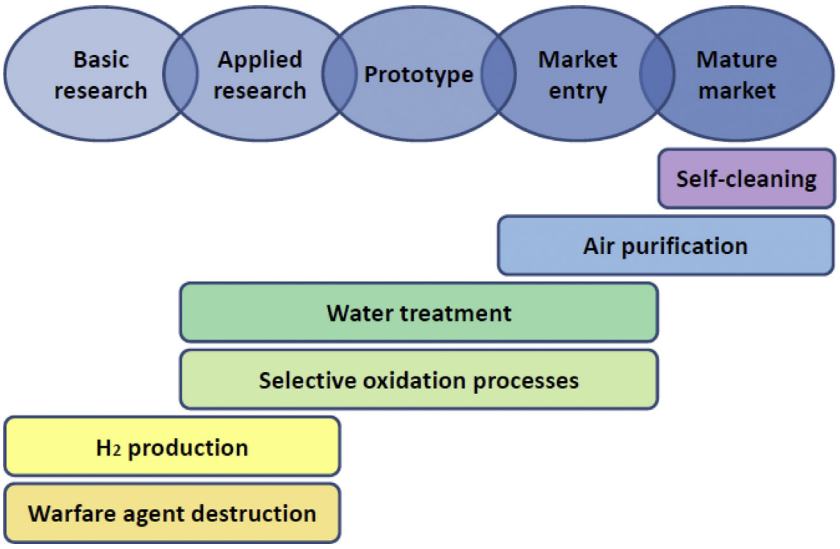

Fig. 3. Photocatalytic technology readiness level (adapted from [137]).

Table 1
Main commercial applications of titanium dioxide with sunlight.

Commercial field	Function	Use
Glass	Self-cleaning, antibacterial, and antifogging	Windows, mirrors, and vehicle glasses
Vehicles	Self-cleaning, antibacterial, antifogging, and avoiding dewdrops	Coating and painting of vehicles, and side-view mirror
Textiles	Self-cleaning and antibacterial	Tent materials, storage structures, and stations and domes
Food and flowers	Antibacterial and anti aging	Fruits and flowers preservation
Buldings, hospitals, and concrete	Self-cleaning, antibacterial, and antifogging	Kitchen, bathrooms, exterior tiles and coating, and walls and roofs
Road materials	Self-cleaning and antifogging	Road pavements and mirrors, sidewalks, and lighting and signs
Water treatment	Decontamination, antibacterial, and mineralization	Small industrial and agricultural wastewater treatment plants
Industrial chemistry	Selective oxidation	Fine chemicals solar productions

2. Photocatalytic technology

The level of development of solar photocatalytic technology varies depending on the field of application, and ranges from basic research to mature market-ready processes (Fig. 3).

Solar photocatalytic applications marketed on different levels (narrow or expanded markets) relate to wastewater treatments, production of selected fine chemicals, air purification (outdoor environments), and self-cleaning materials.

Solar photocatalysis is used to treat vey toxic wastewaters or mineralize, in the presence of oxygen, bio-refractory organic pollutants, especially halogenated compounds:

$$C_xH_yCl_z + \left(x + \frac{y-z}{2}\right) O_2 \xrightarrow{\text{photocatalyst}} xCO_2 + zH^+ + zCl^- + \left(\frac{y-z}{2}\right) H_2O \quad \text{(r5)}$$

The direct use of solar radiation is highly attractive for industrial photochemical production of some fine chemicals. The opportunities for industry are twofold: solar chemical processes can be employed directly in industrialized countries wherever there is enough sunlight available, or they can be exported to industrializing countries with a good solar resource. In this respect, industrial production of ϵ-caprolactam, the preferred monomer for manufacture of nylon-6, by photochemical synthesis is a reasonable reference case showing the energy-saving advantages of solar technology over conventional processes. The Japanese company Toyo Rayon Ltd. was able to produce 160,000 t/year of ϵ-caprolactam (5% of global demand) by artificial cyclohexane photonitrosation in 1991 [59]:

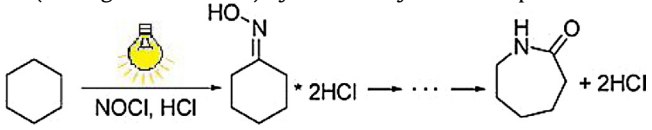

(r6)

Evaluation of the energy demand of industrial solar production of ϵ-caprolactam demonstrated a four-fold lower demand for electricity and an eight-fold lower demand for cooling energy compared to the typical Toray protocol. Moreover, due to avoided conversion of fossil fuel to electricity, the solar process would avoid specific emissions of 1.5–2.5 t of CO_2 per ton ϵ-caprolactam.

The solar photocatalytic technology, mainly heterogeneous with TiO_2 as the photocatalyst, has progressed rapidly, and is used increasingly in the development of construction materials, such as ceramic tiles, paving-blocks, glass, paints, concrete pavements with self-cleaning properties or finishing coatings with air-water purification, and antibacterial roles (Table 1) [60]. TiO_2 photocatalysts have attracted much attention as photofunctional materials for self-cleaning, antifogging, self-sterilizing, and antibacterial agents [12,61].

The widespread use of TiO_2 is attributed to its high catalytic efficiency, chemical stability, economy, low toxicity, and good compatibility with traditional construction materials [61].

Fig. 4. Dives in Misericordia Church in Rome (left); Cité de la Musique et des Beaux-Arts in Chambéry (right).

The synergy of two titanium dioxide's photo-induced properties (photocatalysis and super-hydrophilicity), as described above, is the basis of its self-cleaning ability [62].

2.1. Self-cleaning functions and TiO_2-modified concrete

Among the first products based on solar photocatalysis with titanium dioxide to be marketed were self-cleaning coatings for window glass [63,64] and photovoltaic or solar panels with improved transmittance of natural sunlight (TitanShield™ Solar Coat). In 2001, Pilkington Glass, an affiliate of NSG, manufacturers of glass and glazing systems, announced the development of the first self-cleaning windows, Pilkington Activ™, and later other major glass companies released similar products, including PPG's Sunclean™, Saint Gobain's Bioclean, and Impact Safety Glass.

These products, which consist of a layer of nanocrystalline titanium dioxide (anatase form) a few score nanometer thick deposited by chemical vapor deposition on soda-lime silicate float glass, have high visible transmission and reflectance properties [65].

In practice, cleaning glass surfaces and tiles requires high energy consumption and chemical detergents, and consequently high costs. The inorganic and organic molecules adsorbed on a TiO_2-based self-cleaning surface can be easily degraded and then washed with water due to the high hydrophilicity of titania film. Thus, a fraction of the pollutants, or photo-oxidized byproducts, deposited on the surface can be removed by the cleaning effect of TiO_2 [66]. The final result is "*cold combustion*" surface cleaning, which is the conversion of organic molecules to carbon dioxide, water, and other byproducts, if heteroatoms are present, at ambient temperature.

However, the self-cleaning function is effective only when the flux of the incident solar photons is higher than the rate of adsorption of the organic pollutants on the surface.

About 2×10^4 m^2 of outdoor photoactive self-cleaning glass, manufactured by the Nippon Sheet Glass Co., are installed in the Central Japan International Airport terminal building, which was completed in 2005 [62,67]. The New National Grand Theater of China is also equipped with self-cleaning glass [68].

In addition to glass surfaces, the best use of TiO_2 self-cleaning properties is related to construction and coating materials for walls in buildings, since these materials are exposed to sunlight and natural rainfall.

Most exterior building walls become soiled from automobile exhaust, which contains mineral oils and unburnt components. By coating walls with super-hydrophilic TiO_2, dirt on walls can be washed away by rain, keeping building exteriors cleaner longer [69].

Since the late 1990s, TiO_2-based materials like tiles, aluminum siding, plastic films, fabrics for tents and cements are already being marketed, especially in Japan [62,70]. Some benefits of photocatalytic concrete are that it decomposes chemicals that contribute to soiling and air pollution, keeps the concrete cleaner, and reflects much of the sun's heat, because it is white, thus, reducing heat gain [71].

White cements containing TiO_2 are used for the construction of buildings in Europe too. In 1996, the first real project on the self-cleaning activity of titanium dioxide in cementitious materials was for designing the mix for "Dives in Misericordia" Church in Rome, Italy, and evaluating the self-cleaning ability of a new type of cement (TX Millennium™) [69,72]. The project was completed in 2003 by Italcementi S.p.A., an Italian cement company (Fig. 4, left). Over a six-year monitoring period, only a slight difference was observed between the white exterior and interior Church walls.

Italcementi has developed different types of cement with a titanium dioxide surface, TX Aria™, TX Active™, and TX Millennium™ [73], and used them in many other demonstration projects, like a school in Mortara, Italy (completed in 1999), the Cité de la Musique et des Beaux-Arts in Chambéry, France, completed in 2000 (Fig. 4, right), the Roissy Air France Headquarters at Charles de Gaulle International Airport (Paris), and the Hôtel de Police in Bordeaux. In the Chambery City Hall, the primary color remained almost constant in different facade positions (West/North/East/South) for approximately five years.

They have also been used to check the photocatalytic effects of a TiO_2-coated highway for converting polluting gas emissions, such as NO_x and SO_x, to more environmentally benign forms like nitrates and sulfates [74,75].

TioCem®, manufactured by Heidelberg Cement Technology Center, GmbH, is another photocatalytically-active concrete product containing titanium dioxide which is able to promote catalytic degradation of NO_x and other air pollutants [76]. These photocataytic cements were among Time magazine's top 50 inventions of 2008. By 2003, self-cleaning TiO_2-based tiles had been used in over 5000 buildings in Japan, the most famous of which is the Maru Building, located in Tokyo's main business district [67]. Other examples of Japanese buildings

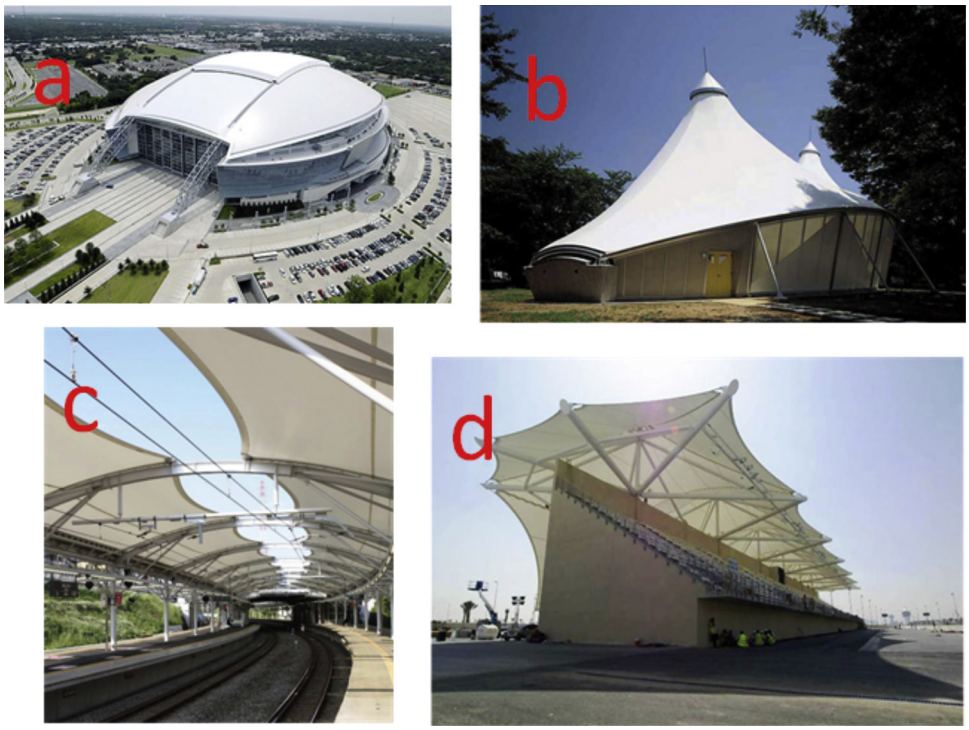

Fig. 5. (a) Cowboy Stadium (Dallas, U.S.), (b) Tokyo University (Japan), (c) Kajigaya Station (Japan), (d) YAS Marina Circuit (UAE). Manufacturer: Taiyo Kogyo Corporation.

with photocatalytic materials are MM Towers in Yokohama, a food processing plant in Saga, and Juntendo and Hokkaido Universities in Tokyo and Hokkaido, respectively.

In Japan, 2003, the sales of photocatalytic construction materials made up 60% of the whole photocatalytic market share and several tall buildings have been covered with thousands of TOTO's self-cleaning tiles [67].

TOTO, Ltd., the pioneer in titania coating self-cleaning technology, the maker of Hydrotect^{TM}, estimates that a building in a Japanese city covered with ordinary tiles should be cleaned at least every five years to maintain its good appearance, while one covered with self-cleaning tiles should remain clean for twenty years without any maintenance, thus, greatly decreasing maintenance costs.

A particularly interesting aspect of titanium dioxide-cement composites is that there is a clear synergy between the cementitious material and TiO_2 that makes cement an ideal substrate for environmental photocatalysis [77,78]. In fact, many photooxidizing compounds, such as NO_x and SO_x have acidic properties and the basic nature of the cement matrix is particularly suitable for fixing both the polluting reagent and the photooxidation products on its surface. These cements are normally loaded with up to 3% w/w of TiO_2 for optimum activation and cost efficiency [78]. TiO_2 photocatalytic surface coatings have been demonstrated to provide acceptable durability and wear resistance [79].

Although no cost data are currently available, they are generally expected to be higher for TiO_2 modified concrete than for conventional concrete. In this regard, a life-cycle cost analysis (LCA) carried out by Churchill and Panesar [80] demonstrated that for a 40-year service life and assuming a 6 mg h^{-1} m^{-2} NO_x degradation rate, a highway noise barrier designed with 100% general-use cement and a photocatalytic concrete cover (25 mm thick), has a 7% and 30% higher annual cost than the 100% general-use cement, and 35% ground granulated blast furnace slag barriers (GGBFS) normally employed as concrete replacement without photocatalytic cover, respectively. Moreover, the use of a photocatalytic concrete cover on cement containing 35 and 50% GGBFS is more economically viable than 100% general use cement, regardless of the lifetime and pollution removal rate.

In addition to cement, other coatings are commonly treated with titania particles, when the coated surface is sufficiently stable to physical (viscosity, flocculation) or chemical change (photodegradation, oxidation, etc.). For example, the "chalking" phenomenon which is the destructive oxidation of commercial polymers containing titania within the near surface layers of the coating under exposure to sunlight [62]. Continuous erosion of the material leaves the pigment particles exposed to weathering [81].

Photooxidation studies on polymeric materials containing nanoparticle and pigmentary-grade titanium dioxide show that in general the first exhibit high photocatalytic activity, promoting the oxidation of the polymer during processing and long-term thermal ageing by generating hydroperoxidic and carbonylic species [82].

Tent materials made from flexible PVC film are usually too difficult to clean. But photocatalytic PTFE and PVC membrane structures using TiO_2 coating technology have recently been demonstrated to possess greater chemical resistence and self-cleaning properties. This technology enables TiO_2 coated membrane structures to maintain their good appearance and light transmittance for a longer time. Self-cleaning tent materials have been widely applied for storage structures, business facilities, bus and train stations, sports arenas, domes, canopies and tents in parks, and at beaches [83,84], thus, saving time and cost of cleaning maintenance (Fig. 5).

Moreover, TiO_2 has been found to be an excellent photocatalyst for use in pavement engineering for reducing polluting vehicle emissions [85].

Since titanium dioxide, when exposed to natural sunlight, is able to remove nitrogen oxides in exhaust from vehicles in metropolitan areas (photo-de-NO_x process) [86,87], some companies are using TiO_2 photocatalysts in paving materials, and TiO_2-coated paving stones over pavement have become available on the market. On the basis of the above, numerous photocatalytic cementitious materials have

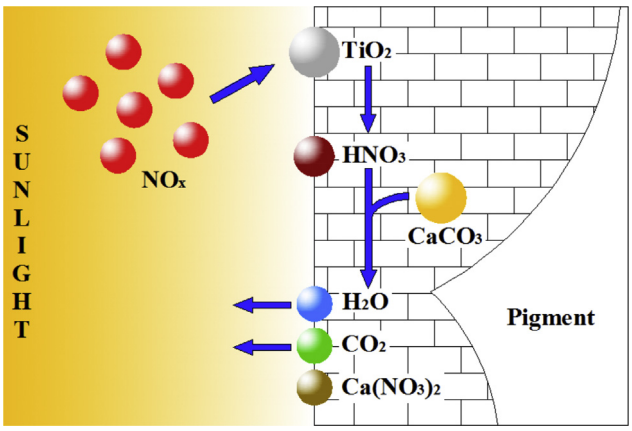

Fig. 6. Capturing energy from sunlight to neutralise vehicle pollution.

been patented [72,88–91], although the effectiveness of titania mixtures and their influence on overall photocatalytic performance still lacking systematic research [92]. In particular, TiO_2 high-porosity cementitious composites have high NO_x degradation rates [93,94].

Japan's Mitsubishi Materials Corp., developed a paving stone called NOxer^{TM} which they have tested in Osaka, Chiba, Chigasaki & Saitama-Shintoshin [89]. NOxer^{TM} makes use of the catalytic properties of TiO_2 to remove nitrogen oxides, mainly from vehicle emissions, from the air, converting them into more ecofriendly molecules that can be washed away by rainwater [95].

When the surface of the NOxer^{TM} material is illuminated, the oxygen created oxidizes NO_x into nitric acid which can then be washed away by rainfall or neutralized by the alkaline composition of the concrete (Fig. 6).

TiO_2 paving stones have been tested on about twenty roads (more than 50,000 m^2) in Japan over the past ten years. One of the places tested is a 300 m^2 area on Belt Highway No. 7 in Tokyo. Nitrogen oxides removed from this test area were estimated to be 50–60 mg day^{-1}, the NO_x load discharged by 1000 vehicles [93].

Hamada et al. [96] showed that TiO_2 materials applied in airports, including Tokyo International Airport (Haneda Airport) and Ishigaki Domestic Airport (Okinawa Prefecture), lowered NO_x by 10–30%. Some estimates of NO_x removal (50,000 t $year^{-1}$), evaluated using photocatalytic pavements for five years, are very promising [97].

In Europe, some demonstration projects done by Italcementi have also confirmed the ability of titanium-dioxide cement (TX Aria) to destroy automotive gas emissions. These projects involved repaving Borgo Palazzo Street in Bergamo (Italy), Modigliani Street in Segrate (Italy), and Jean Bleuzen Street in Vanves, near Paris (France) [98].

Impresa Bacchi (Italy) has developed a photocatalytic technology for preparing a water emulsion with titanium dioxide that is sprayed onto asphalt pavement surfaces located in very polluted areas.

The asphalt pavement in the Rogoredo auto-park in the outskirts of Milan (4000 m^2) and the SP70 road in the province of Forlì–Cesena (2500 m^2) were treated with water–TiO_2 emulsions, achieving high photocatalytic NO_x elimination efficiencies [99].

Interesting examples of pedestrian sidewalks made with TiO_2-containing permeable blocks or TiO_2-containing adsorbents as decorative elements located in open-spaces where sunlight is available, such as balconies and terraces, have been described [100].

Extensive large-scale research on NO_x photoelimination carried out at the European Photoreactor (EUPHORE) in Valencia, Spain (Fig. 7) is worth noting. The EUPHORE photoreactor consists of two outdoor 200-m^3 hemispherical Teflon chambers that transmit over 80% of the natural sunlight. The chambers are equipped with sensors and analytical devices for detection of trace substances, such as spectrometers, on-line monitors for ozone and NO_x, and several GC and HPLC systems. Sunlight intensities are measured with spectral radiometers [101]. The EUPHORE reactor has been used to study the synergic reactions of NO_x, alifatic and aromatic hydrocarbons, ozone, and other

Fig. 7. European Photoreactor (EUPHORE), with some of the instrumentation located inside the chamber. In addition, sampling ports for on-line and off-line instruments are situated in the central flanges (photo: Euphore website, directly cited).

gaseous pollutants under solar irradiation [102,103]. Another function related to the photo-induced hydrophilicity of TiO_2 is its antifogging effect. Mirror surfaces fog up when steam cools down on these surfaces forming aqueous droplets. Many Japanese cars are equipped with super-hydrophilic antifogging and self-cleaning side-view mirrors [50,104].

2.2. Bactericidal (mildew-proof) coating

Titania and metal-doped titania coatings can not only inhibit the reproduction of bacteria, but also decompose the bacterial cells at the same time [105–107]. Thus, application of TiO_2 materials in hospitals and health care facilities, such as public lounges, have recently attracted the attention of both academia and industry [108]. Nanostructured crystalline titanium dioxide coatings deposited by cathodic arc evaporation on five medical implant-grade titanium substrates demonstrated UV-induced photocatalytic activity that can provide bactericidal protection against *Staphylococcus epidermidis*. These results and those of other studies are encouraging the development of antimicrobial surfaces in orthopedics and dentistry to prevent or treat post-surgical infection [109].

One of the most widely used applications of photocatlytic materials is for their antimicrobial property in interior paints. These paints are formulated with aqueous acrylic dispersion, rutile titanium dioxide, extenders, and special additives, such as photocatalytic nano zinc oxide and different types of photocatalytic anatase titanium dioxide. The paint containing a mixture of the first type of TiO_2 and nano-ZnO have shown the best photocatalytic antimicrobial effect. They have been demonstrated for *Escherichia coli*, *Staphylococcus aureus*, *Pseudomonas aeruginosa*, fungi *Aspergillus niger*, and *Penicillium chrysogenu* [110].

The first photocatalyst coating was made by the Japanese Arc-Flash Company in 1992 using photocatalyst fixation technology, sprayed directly on the surface. The Arc-Flash® photocatalyst coating, using titania nanoparticles as the main ingredient, can effectively sterilize mildew, sanitize enviroments, such as hospitals, residential kitchens, schools, and floors, killing bacteria with over 98% efficiency and improving hygiene standards [111]. Moreover, the photocatalytic and antibacterial properties of the Arc-Flash® photocatalyst may reduce the spread of infection to hospital patients, especially those with a weak immune system.

2.3. Preservation of perishable goods

In addition to the solar applications described above, TiO_2 may be used to treat the air in fruit, vegetable, and cut flower storage areas to prevent spoilage and increase product shelf life. The Kennesaw, Georgia-based KES Science & Technology Inc. (GA, USA), Catalyx Technologies, LLC, (PA, USA) and ABSOGER Sas Co. (Les Barthes, FR) have marketed enclosed systems called "Bio-KES", "AiroCide®", "FRESH+™" and "ABSOGER", respectively, which make use of the photocatalytic properties of TiO_2 for the destruction of gas-phase ethylene to prevent premature fruit maturation [112–114]. Ethylene is a gaseous growth hormone produced naturally by plant tissue which in concentrations as low as 1 ppm triggers the ripening of fruits and vegetables. Originally developed by NASA to keep the air clean onboard the International Space Station and aboard the space shuttle [115], the "Bio-KES" and "AiroCide®" technologies break down ethylene into CO_2 and water:

(r7) $$C_2H_4 + 3O_2 \xrightarrow{TiO_2,\ h\nu} 2CO_2 + 2H_2O$$

The "Bio-KES", "AiroCide®", "FRESH+™" and "ABSOGER" systems are currently employed by florists and fruit merchants to keep produce fresh longer, slow wilting of flowers and eliminate growth of mold on fruits.

3. Solar photocatalytic chemical production and wastewater treatment

The use of homogeneous and heterogeneous solar photocatalysis for synthesis of fine chemicals and wastewater treatment is gaining interest. In fact, the use of solar energy in chemical production or in treatment of urban and industrial effluents could be an effective, economical solution to several environmental problems.

3.1. Design of solar photocatalytic reactors for commercial use

Any industrial application of a photocatalytic process requires a photoreactor, that is, a specific device which can efficiently bring solar photons and chemical reagents into contact with the photocatalyst. Solar photoreactors differ significantly from classic chemical reactors in that their physical geometry is of critical importance in ensuring that solar radiation is efficiently collected. In this sense, conventional operating parameters, such as temperature, pressure, and mixing may be less important for the purposes of optimal photocatalytic process operation. However, it should be noted that for the photo-Fenton process the effect of the reaction temperature caused by the Fenton thermal reaction can be important on the reactor performance [116].

With a heterogeneous catalyst, one of the major problems in the design and scale-up of a solar photoreactor is achieving uniform distribution of sunlight inside the reactor, due to absorption, reflection, and scattering effects by the catalyst particles or the supporting material. Poor distribution of the solar radiation entering the reactor leads to lower overall efficiencies of the photochemical process. In fact, if the catalyst load is too high, the resulting turbidity keeps enough sunlight from penetrating inside the reactor.

On the other hand, a homogeneous photocatalyst absorbs the solar energy depending on its molar absorptivity and this has to be taken into account when estimating the optimal concentration of the catalyst with respect to the photoreactor light-path length.

Another important factor related to a natural solar photoreactor design is its optical-path length (OPL), since it must be ensured that it is uniform for both the flow and distribution of the photon flux at all times, everywhere inside the reactor. When suspended heterogeneous photocatalysts are employed, turbulent flow must be ensured to prevent particle deposition phenomena in the hydraulic circuit. But turbulent flow causes loss of pressure, a critical parameter that can affect scale-up, especially in the case of long photoreactor lengths. An OPL below 20–23 mm is not feasible due to pressure loss, whereas, over 50–55 mm is impractical for constructing photoreactors with sufficient pressure resistance without making glass walls too thick [117].

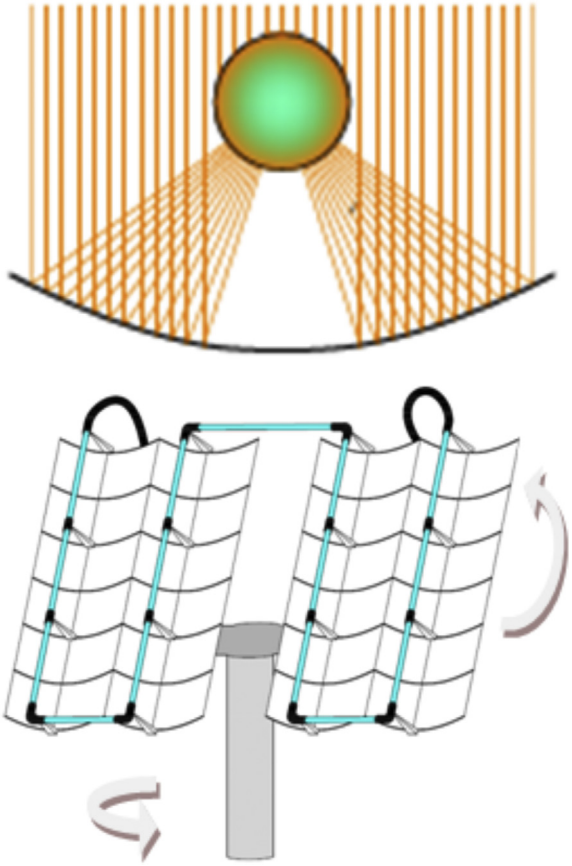

Fig. 8. Behavior of incident solar radiation on a PTC (up) and PTC solar photoreactor (down). (For interpretation of the references to color in this text, the reader is referred to the web version of this article.)

There are some critical reviews in which the design parameters and performance of the more common pilot and commercial-scale photoreactors are discussed and compared [116,124,125]. Most solar photoreactors can be divided into three different families:

- Parabolic trough collectors (PTCs).
- Non-concentrating collectors (NCCs).
- Compound parabolic collectors (CPCs).

3.1.1. Parabolic trough collectors

The PTC engineering concept came from solar thermal energy production applications [126]. They consist of reflective, parabolic surfaces that concentrate the solar radiation on a transparent tube along the parabolic focal line through which the reactant fluid flows (Fig. 8). The platform usually has two motors controlled by a two-axis (azimuth and elevation) tracking system. Thus, for maximum efficiency, the collector aperture plane is always perpendicular to the solar radiation, which is thus, reflected by the parabola onto the reactor tube (light blue zone in the figure).

The concentration factor (CF) of the solar collector is defined as the ratio between the collector "aperture area" and "absorber area". The "aperture area" is the area that intercepts the solar radiation and the "absorber area" is the area of the component that receives the sunlight. For photocatalytic applications with PCT reactors, the concentration factor ranges from 5 to 35 suns [18,127].

The trough surfaces are usually aluminum to ensure the highest reflectivities. The system supports turbulent flow with efficient homogenization. Some overviews on commercial parabolic-trough collectors designed for supplying thermal energy are also available [125,126].

The reactor tube is a closed system, preventing vaporization of volatile compounds. The photocatalyst is generally suspended in the fluid although some designs for a supported photocatalyst have been studied [53].

The major advantage derives from the increased intensity of the incident radiation, which allows smaller photocatalyst loads than other photoreactors with the same solar light collecting area. This results in smaller receiver tube diameter requirements, which in turn means operating pressures can be higher and construction material quantities lower.

The main disadvantages are that, because of their geometry, the collectors can use only direct beam radiation, making them practically useless on cloudy days, their tracking system makes them more expensive, and quantum efficiencies are low due to high electron/hole recombination [18]. Moreover, for intermediate and high solar zenith angles, the diffuse component in the UV solar spectrum may be equal to or greater than the direct component of UV solar radiation, even for cloudless days [128].

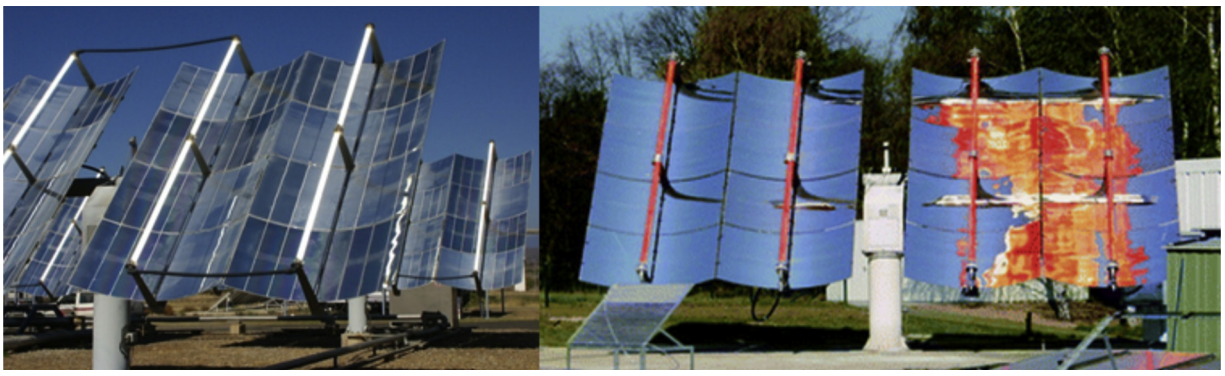

Fig. 9. (left) SOLARIS loop with two-axis tracked parabolic trough collectors concentrate solar radiation for chemical processes (source: www.volker-quaschning.de); (right) PROPHIS loop with line-focusing parabolic mirrors (left three troughs) and reflection holograms (right trough) (*with permission of RSC*).

However, high capital and operating costs from the mechanical complexity of PTCs are expected to drop as innovative tracking mechanisms and processes are further developed [124]. The PTC capacity to concentrate solar radiation may cause the reactor to overheat and increase the photogenerated e_{CB}^{-}/h_{VB}^{+} recombination reaction rates if heterogeneous metal-oxide photocatalysts are used, thus, reducing process efficiency.

As mentioned above, the first PTC was installed in Albuquerque (New Mexico, USA) in 1989, and consisted of six aligned parabolic-trough collectors with single-axis solar tracking, an aperture of 2.13 m and a length of 36.4 m, for a total area of 465 m^2. The collector concentrated the sunlight about 50 times on the photoreactor, which was designed for photocatalytic treatment of polluted water containing chlorinated solvents and heavy metals [23,129].

PTC reactors were later adapted specifically for solar photocatalytic applications at the Plataforma Solar de Almeria (PSA) in Spain (Fig. 9, left) and at the German Aerospace Centre (DLR) in Cologne, Germany (Fig. 9, right), where laboratory, preindustrial, and industrial-scale experiments in production of fine chemicals can be carried out. The SOLARIS and PROPHIS (Parabolic tRough collector for Organic PHotochemical syntheses In Solar light) loops, with a 35–120 L reaction mixture capacity, are used for industrial reactions.

Each SOLARIS and PROPHIS collector consists of a turret, a crossbeam, four troughs, piping and electrical equipment, and a two-axis solar tracker to align the collector with the Sun's position. Direct solar radiation strikes the rectangular collector aperture and the parabolic mirrors reflect the radiation into the transparent receiver–reactor tubes which are positioned in the four focal lines. The reaction mixture is pumped through the receiver–reactor tubes connected in series until the desired conversion has been achieved. In an external heat exchanger, excess heat is removed and rejected to the ambient by an air cooled process cooler [59].

These parabolic-trough collectors were initially designed to transform solar radiation into thermal energy and were later transformed for photochemical applications [24].

The concentrating power is about 30–32 suns. They can achieve a productivity up to 1000 kg $year^{-1}$ with product quantum yields in the range of 0.5–0.8, and products up to a molecular weight of about 100 u.m.a [130].

Use of SOLARIS and PROPHIS PTCs for the synthesis of fine chemicals has been described. One of the first important industrial processes was the solar photooxygenation of citronellol with singlet oxygen sensitized by Rose-Bengal in isopropanol. The product mixture, after a reduction with sodium sulfite, contains Rose Oxide (yield 55%), an important fragrance, over 100 t of which is currently produced annually with sunlight [131]:

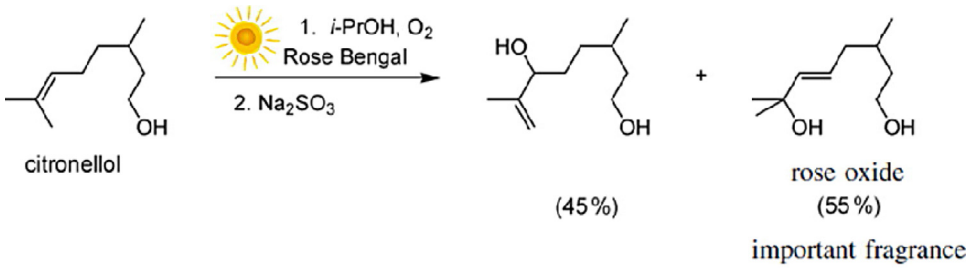

(r8)

A solar plant manufacturing Rose Oxide in Central Europe is up to 11% more lucrative than conventional production, reducing the manufacturing costs of Rose Oxide to $1.60/kg [132].

Application of the SOLARIS reactor for synthesis involving photooxidation of furfural sensitized by Rose-Bengal or Methylene Blue to yield 5-hydroxyfuranone, a versatile C_4 building block, has also been reported [133]:

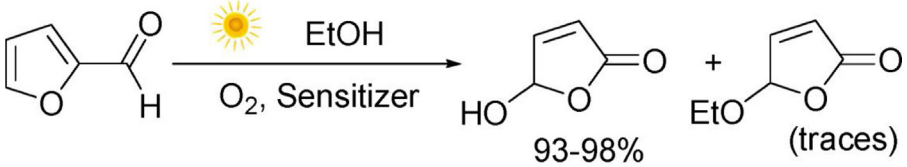

(r9)

Another interesting application of solar radiation is the production of juglone (5-hydroxy-1,4-naphthoquinone), a coloring agent for foods and cosmetics and versatile biologically active quinone, by Rose-Bengal or Methylene Blue-sensitized photooxygenation of 1,5-dihydroxynaphthalene under a stream of oxygen using isopropanol as solvent [134]:

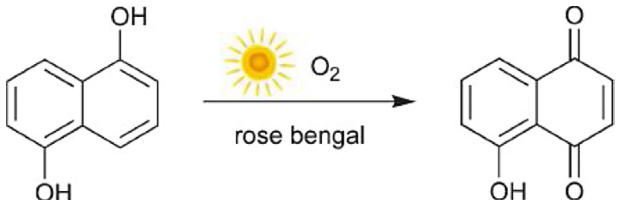

(r10)

Acceptable multi-gram juglone yields of up to 79% are achieved after just 4 h of illumination in a PTC reactor equipped with holographic concentrators designed to reduce warming caused by the infrared solar radiation, and thereby cut cooling costs. Under these adapted outdoor conditions, the solar process has been demonstrated to be a valid alternative to existing conventional processes [135].

The PROPHIS plant was also employed for the synthesis of 2-alkyl and 2-aryl pyridines, which are bulk chemicals and precursors of biologically active compounds. The cyclization of ethyne and nitriles, photocatalyzed by $(C_5H_5)Co(C_2H_4)$ yielded over 98% of the desired product [136]:

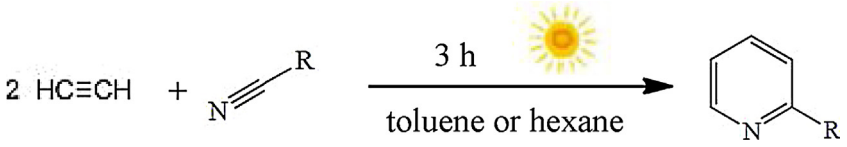

(r11)

The heterocyclization of ethyne with benzonitrile in a toluene-water mixture under argon atmosphere and in the presence of $(C_5H_5)Co(C_8H_{12})$ as the catalyst yielded 40% 2-phenyl-pyridine after 5 h of solar illumination [130]:

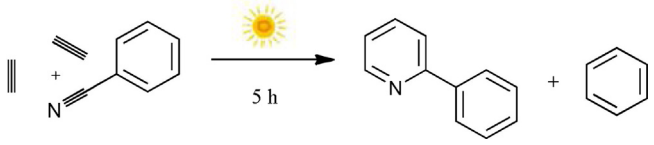

(r12)

A solar photoinduced acylation reaction of quinones and naphthoquinones was carried out in the PROPHIS facility producing 90% half-kilogram yields of acylated derivatives, which are versatile synthones for the synthesis of tetracycline [138]:

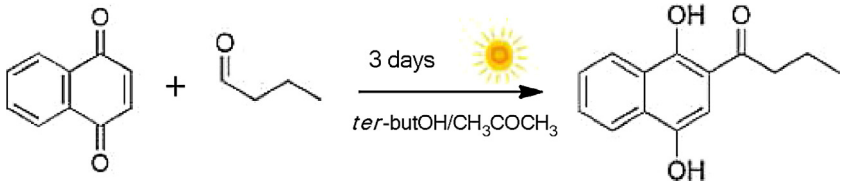

(r13)

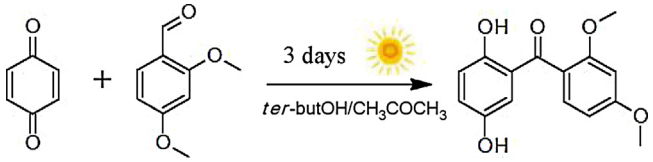

(r14)

Biorecalcitrant water has been treated in a solar TiO_2-based photocatalytic plant with 158 m^2 of parabolic-trough concentrator collectors installed at Lawrence Livermore National Laboratory, in Livermore, California (USA). The plant was used for chemical treatment of groundwater contaminated with trichloroethylene [139].

3.1.2. Non-concentrating collectors

The non-concentrating (NCC) or inclined plate collector (IPC) is a flat or corrugated inclined plate over which the fluid flows in a thin film. The photocatalyst is usually supported on the surface of the inclined plate, with the photons first traveling through the reactant fluid before reaching the photocatalyst (Fig. 10). The back plate may be glass, metal, or stone. As the solar radiation is not concentrated, this reactor design is able to capture diffuse light.

The top may also be left open to the atmosphere, further increasing efficiency by excluding light absorption by the reactor cover and removing the potential for a suspended photocatalyst to form an opaque film on its inner surface. In this case, the main drawback may be high volatile chemical and water losses by evaporation and interference from the atmosphere [19]. It could also be dangerous under windy conditions when wastewater to be treated is toxic.

The thin-film fluid, typically in the range of 100–200 μm, requires a relatively low flow rate to be maintained on the bottom surface. Normally, the specific flow rates are in the range of 0.15–1.0 L min^{-1} m^{-2}. With higher flow rates, reactor residence times are shorter and film thickness increases, thus, leading to increased mass-transfer constraints and a decrease in NCC efficiency.

NCCs collectors, due to their design simplicity (staticity) and low capital costs (no moving parts or tracking mechanisms) [140], have been demonstrated to be effective for small-scale operations, particularly in less developed regions where other wastewater treatment plants are unfeasible.

However, non-concentrating reactors require larger surfaces than the concentrating photoreactors and, therefore, must be designed to resist the high operating pressures necessary to be able to pump the fluid, substantially increasing their cost [141].

NCCs are mainly used in solar pilot plants for the photocatalytic treatment of various industrial or agricultural wastewaters containing bio-refractory organic pollutants [142–144] and for agroindustrial water disinfection using a heterogeneous catalyst [145].

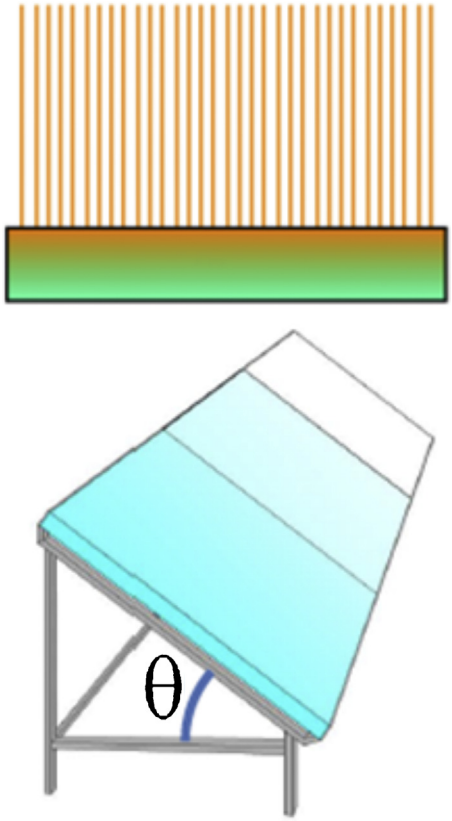

Fig. 10. Behavior of incident solar radiation on a NCC (up) and NCC solar photoreactor (down).

In 2004, 2.5 m-wide by 10 m-long solar photocatalytic NCC reactors using TiO_2 with a total illuminated area of 50 m^2, oriented to the South and tilted 20°, were combined with two 15 m^3-capacity bioreactors used for pretreating the effluents, and installed at a Tunisian textile mill (Menzel Temime) for decoloration of wastewater [146].

Some applications in presence of a homogenous catalyzed process, i.e., photo-Fenton, have also been reported [147].

An NCC reactor has been used in Germany for photosensitized cyclization of 1,1-dicarbonitrile using 1,4-dicyano-2,3,5,6-tetramethylbenzene (DCTMB) as the electron acceptor [148]:

(r15)

The results, collected under partly sunny or cloudy conditions, demonstrate higher NCC reactor efficiency than with a PTC, probably due to the high percentage (40%) of diffuse radiation in the solar radiation incident in central Europe.

3.1.3. Compound parabolic collectors

Compound parabolic collectors (CPCs) are an interesting cross between PTC and NCC photoreators and are a good solution for solar photochemical applications [18]. CPCs are stationary collectors with a parabolic reflective surface around a cylindrical reactor tube (Fig. 11).

The main advantage of a CPC is that the reflector geometry reflects indirect light onto the receiver tube, and can therefore, capture both direct and diffuse sunlight [149,150].

The concentration factor and acceptance angle of a CPC are directly related as follows:

$$(eq2) \qquad \mathrm{CF} = \frac{1}{\mathrm{Sin}\theta} = \frac{a}{2\pi R}$$

where θ is the acceptance angle, a the width of the reflector aperture, and R the radius of the receiver. Thus, a CPC with a concentration factor equal to one sun (no concentration) has a 90° acceptance angle. That is, all solar light entering the aperture (both direct and diffuse) is reflected onto the reactor tube.

The total amount of sunlight absorbed in a CPC reactor is much higher than in a PTC, so photoreactors can be smaller and can also be used on overcast days when there is not much direct natural sunlight. Moreover, solar trackers are not required, which significantly reduces system complexity and costs.

Demostration and pilot-scale CPCs with collector areas ranging from 3 m^2 to 150 m^2 (Fig. 12), have been used for homogeneous and heterogeneous photocatalytic removal of very toxic compounds, such as cholophenols, pathogenic organisms [149,151], dyes [152], pesticides [153], chlorinated solvents [154], bacteria [155], and biorecalcitrant compunds [156,157] from water. Other CPC applications include treatment of sanitary landfill leachate [158], olive mill waste [159], and urban wastewater [160].

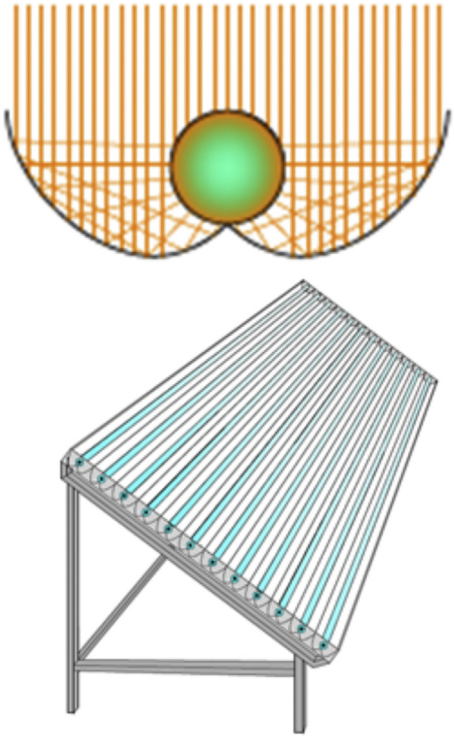

Fig. 11. Behavior of incident solar radiation on a CPC (up) and CPC solar photoreactor (down).

Solar homogeneous (photo-Fenton) and heterogeneous (TiO_2) photocatalytic wastewater treatments have been designed by a European industrial consortium called SOLARDETOX and installed in several different places in Spain [161,162]. These demonstration plants, using photocatalytic CPC reactor modules with photon collection areas of 100–150 m^2, can treat large volumes (m^3) of contaminated water in a few hours.

Since 2007, a homogeneous solar photocatalytic CPC plant (100 m^2) for the pretreatment of saline industrial wastewater containing bio-refractory pharmaceuticals has been operating at a Spanish pharmaceutical company (DSM DIRETIL). The system is able to remove 50% of the initial dissolved organic carbon, and the remaining 45% is removed by an aerobic biological treatment [163].

CPCs for solar production of fine chemicals have been installed for "gram-per-day" or "kg-per-year" reactions. For example, the SOLFIN (SOLar synthesis of FINe chemicals) CPC facility, employed sunlight at a low concentration factor (CF = 2–3 suns) [164]. The SOLFIN apparatus is a 1 m long and 0.2 m wide CPC photoreactor in which the solution volume (up to 25 L) is circulated by a centrifugal pump. The heat generated is discharged by a cooling system to keep the temperature of the reaction mixture below 20 °C.

The reactors have been tested, producing precursors and additives in the industrial synthesis of polymers, pyrethrin insecticides, and pharmaceuticals in the presence of several different photocatalysts, such as titanium dioxide or decatungstate-anions [165].

The SOLFIN facility, for example has been used for 10-gram-scale production of terebic acid, an important industrial intermediate, starting from maleic acid and isopropanol in the presence of water, using benzophenone disodium disulfonate as the photocatalyst. An 83% yield was gained after 14 h of exposure to sunlight [165]:

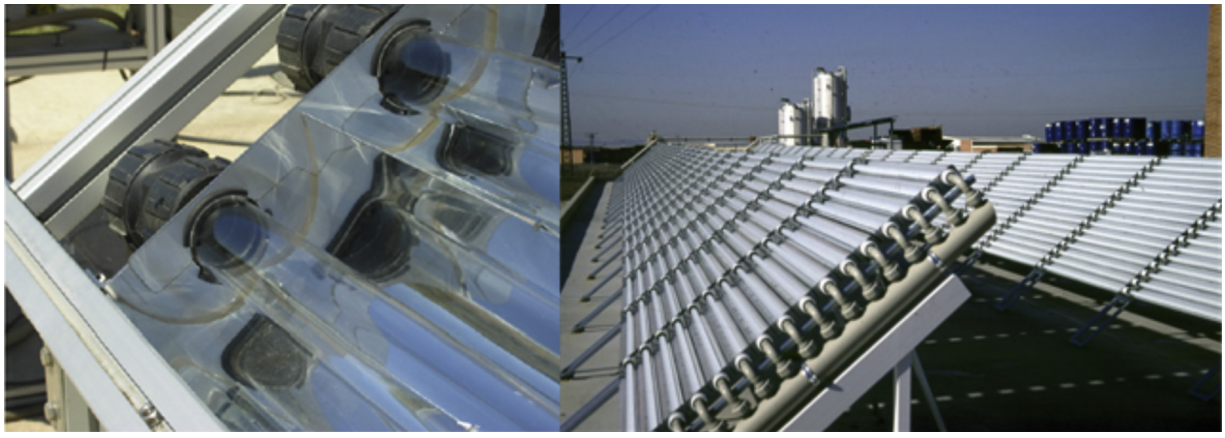

Fig. 12. Partial views of CPC used for solar photocatalytic water detoxification (*with permission of Elsevier*).

Table 2
Comparison of advantages and disadvantages of PTC, NCC, and PTC reactors.

PTC		NCC		CPC	
Smaller reactor volumes	Higher costs (sun tracking)	No optical losses and high optical efficiencies	Large reactor volumes	Smaller reactor volumes	Moderate capital cost
Higher flow rates	Direct solar beams	Low costs (no reflective surfaces)	Pressure limitations	Higher flow rates	Moderate heat generation
Better mass transfer	Optical losses	Simple design (no tracking parts)	Low mass transfer (Laminar flow)	Better mass transfer (turbulent flow)	Difficult to scale up
Low catalyst load	Overheating	Direct and diffuse solar beams	Reactant evaporation (if open)	Direct and diffuse solar radiation	–
Smaller reactor area	Low efficiency	No heating	–	Low catalyst load	–

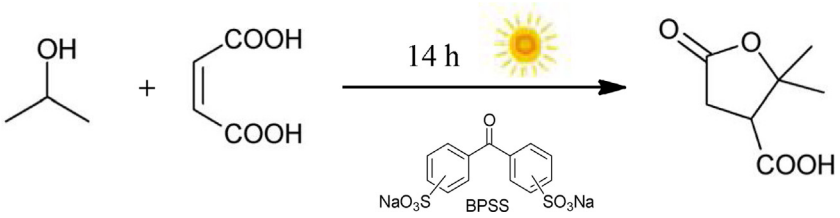

(r16)

1,3-Dioxolane has also been added to, β-unsaturated aldehydes in the SOLFIN plant under the same conditions, producing monoprotected aldehyde yields ranging from 31% to 55% [165].

Moreover, the SOLFIN facility has been used to study the parameters affecting scale-up of selected organic chemical processes [35].

The possibility of producing benzaldehyde, an important ingredient in the manufacture of aromas and flavors, by selective TiO_2 photocatalytic oxidation of benzyl alcohol, has been demonstrated in aqueous solution under natural solar radiation at pilot plant scale in a CPC reactor [2]:

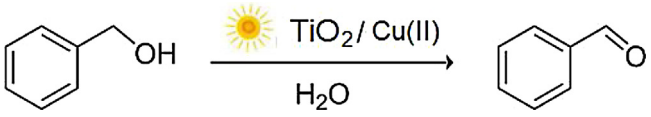

(r17)

The best benzaldehyde yields found were 53.3% for the starting benzyl alcohol concentration (63.4% selectivity) with accumulated energy of 78.9 kJ/L and operating at an average temperature of 38.6 °C.

Such research has clearly demonstrated that some fine chemicals, in particular, valuable substances (>\$100 kg^{-1}) produced in small amounts (<100 t $year^{-1}$) may be synthesized by solar photoreactors, such as CPC collectors.

The main advantages and disadvantages of the reactors described are summarized in Table 2. Several, small or multi-gram-scale studies in bottles, flasks, and glass pipes located on a window ledge, have demonstrated that combining homogeneous or heterogeneous photocatalysis and non-concentrated sunlight is a good method of organic synthesis (alkylation and acylation, cyclisation and cycloaddition, selective oxidation, etc.) for the production of bulk and fine chemicals (Table 3), and reaction yields may theoretically be increased by scaling up PTC, NCC, or CPC reactors for industrial use [166].

4. Solar photoreactors materials, efficiency, and costs

As the reactor walls must be able to transmit solar radiation, materials must be transparent, consequently leading to size limitations, sealing problems, and risk of breakage.

The choice of materials that are transparent to sunlight, and at the same time resistant to aging by it, is limited. Common materials that meet these requirements are fluorinated and acrylic polymers and several types of glass. In particular, fluoropolymers are a good choice of materials due to their high UV-light transmittance, UV, and chemical stability. However, to gain the required minimum operative pressure resistance, the fluorinated wall thickness of the photoreactor has to be increased, thus, decreasing the UV transmittance [167].

Quartz has excellent UV transmittance, as well as good thermal and chemical resistance, but its high cost makes it completely unfeasible for large-scale solar photocatalytic applications. A standard glass cover is insufficient, because it adsorbs part of the near UV solar radiation that reaches the photoreactor surface due its high iron content. However, low-iron borosilicate glass has good transmittance in the solar range to about 285 nm (Pyrex or Duran glass) [117].

Moreover, when glass is exposed to UV-solar radiation, it undergoes aging processes that reduce its UV transmittance. This phenomenon, called "ultraviolet solarization", is attributed to the valence changes in metal ions in the glass, mainly iron (Fe^{2+} transforms into Fe^{3+}) which absorbs UV light. One way to reduce this negative effect is to add 0.1% Si to the glass during melting [118]. As a result, glass transmittance in the 300–400 nm region can only be optimized by strongly reducing the iron content to less than 100 mg kg^{-1}. The German company Schott–Rohrglas GmbH, has developed a borosilicate glass with an iron content of a little over 50 mg kg^{-1} and remarkable transmissivity within the UV range of over 50% at 300 nm [117].

An additional aspect which limits the efficiency of the photocatalytic reactor is so called "window fouling" problem, produced by the photocatalyst sticking on reactor surfaces. The adhesion of a few commercially available powders of TiO_2 on the reactor window can produce an important reduction of the radiation flux entering the photocatalytic reactor [119].

The best choice for the reflecting/concentrating panels is aluminum, because of its very low cost and higher UV-solar reflectivity than silver-coated mirrors. Most piping may be made of polyethylene or polypropylene, however, the use of metals that could be damaged by

Table 3
Selection of photocatalyzed solar organic synthesis.

Photocatalytic alkylation					
Reaction	Product and use	Photocatalyst	Solvent	Yield (%)	Ref.
	Alkylated nitriles	Tetrabutylammonium decatungstate	Acetonitrile	53	[178]
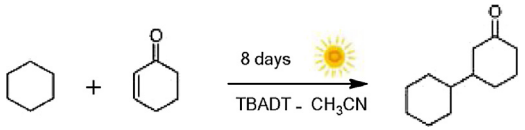	Ketones	Tetrabutylammonium decatungstate	Acetonitrile	40	[178]
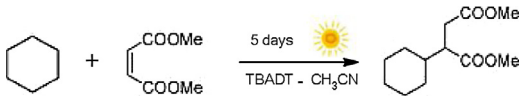	Esters	Tetrabutylammonium decatungstate	Acetonitrile	68	[178]
	Esters	Tetrabutylammonium decatungstate	Acetonitrile	43	[178]
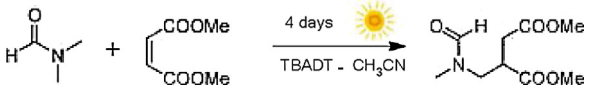	Amido-esters	Tetrabutylammonium decatungstate	Acetonitrile	64	[178]
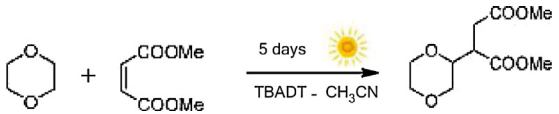	Esters	Tetrabutylammonium decatungstate	Acetonitrile	59	[178]
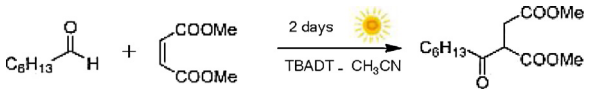	Keto-esters	Tetrabutylammonium decatungstate	Acetonitrile	90	[178]
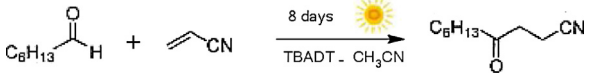	Keto-nitriles	Tetrabutylammonium decatungstate	Acetonitrile	72	[178]
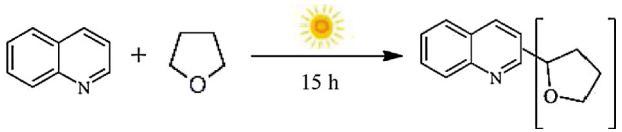	Functionalisation of quinoline	Titania (anatase)	Acetonitrile/H_2O_2	75	[179]
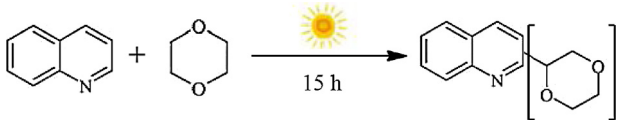	Functionalisation of quinoline	Titania (anatase)	Acetonitrile/H_2O_2	26	[179]

Table 3 (*Continued*)

Photocatalytic alkylation					
Reaction	Product and use	Photocatalyst	Solvent	Yield (%)	Ref.
	Functionalisation of heterocyclic bases	Titania (anatase or rutile)	Acetonitrile/H_2O_2	31–29	[179]
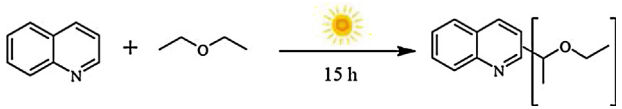	Functionalisation of quinoline	Titania (anatase)	Acetonitrile/H_2O_2	45	[179]
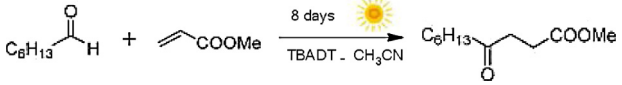	Keto-ester	Tetrabutylammonium decatungstate	Acetonitrile	70	[166]
	Keto-ester	Tetrabutylammonium decatungstate	Acetonitrile	65	[166]
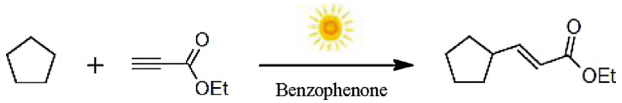	Unsaturated esters	Benzophenone	Cycloalkane	26	[180]
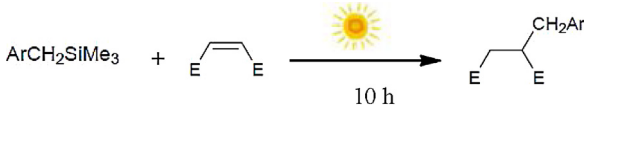	Benzylated succinic acids or anhydrides	Titania	Acetonitrile	65	[181]
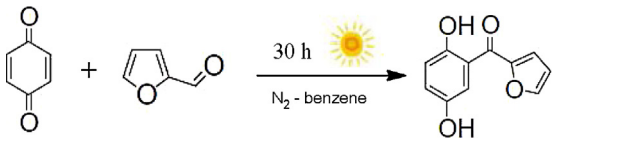	Biologically active quinonoid compounds	–	Benzene	88	[182]
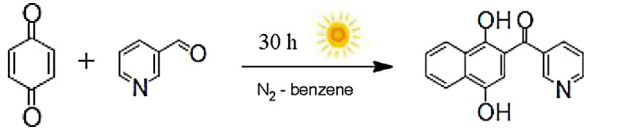	Biologically active quinonoid compounds	–	Benzene	80	[182]

Table 3 (*Continued*)

Photocatalytic alkylation					
Reaction	Product and use	Photocatalyst	Solvent	Yield (%)	Ref.
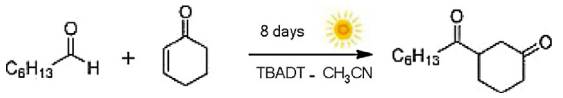	Diketones	Tetrabutylammonium Decatungstate	Acetonitrile	88	[166]
	Functionalisation of some heterocyclic bases	Titania (anatase)	Acetonitrile/H_2O_2	15–88	[183]
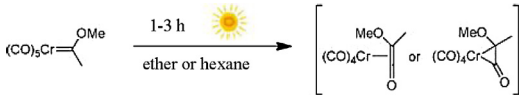	Precursors of β-lactams	Chromium carbenes	Ether or hexane	52–76	[184]
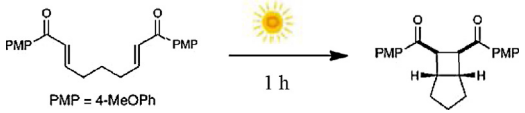	Bicyclic dione	$Ru(bipy)_3Cl_2$, $liBF_4$ and i-Pr_2NEt	Acetonitrile	94	[185]
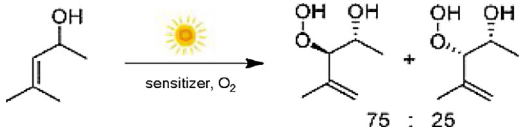	Artemisinine analogues with antimalarial activity [Hoffmanm, 2008]	Tetraarylporphyrine on polystyrene	Solvent less	95	[186]
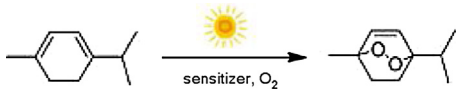	Ascaridole, antimalarial activity [Hoffmann, 2008]	Alkene	Solvent less	–	[187]
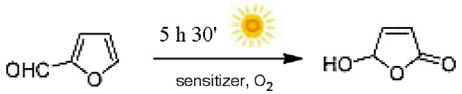	C_5 building block for synthetic use [Hoffmann, 2008]	Rose-Bengal or methylene blue	Methanol	69–94	[188]
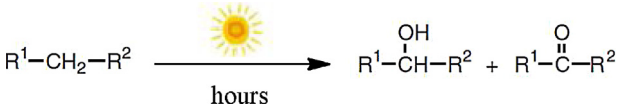	Aldehydes and ketones	$CuCl_2$ or $FeCl_3$	Acetonitrile	>30	[189]

Table 3 (*Continued*)

Photocatalytic alkylation					
Reaction	Product and use	Photocatalyst	Solvent	Yield (%)	Ref.
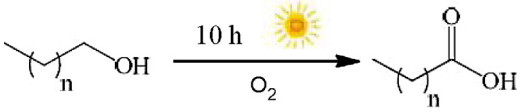	Organic acids	Amberlyst 15, NaBr	Ethyl acetate	62–97	[190]
n = 2, 4 or 6 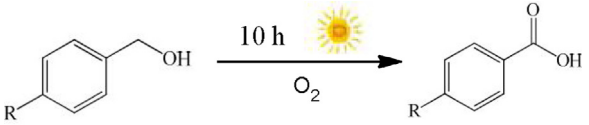	Organic acids	Amberlyst 15, NaBr	Ethyl acetate	95–99	[190]
R = *t*-Bu, Cl 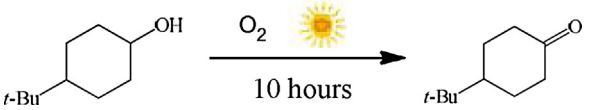	Ketones	Amberlyst 15, NaBr	Ethyl acetate	21	[190]
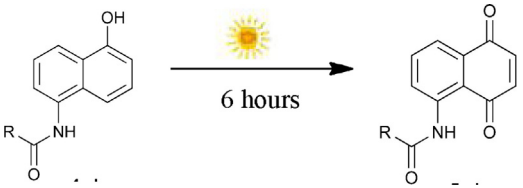	Valueable building blocks in synthesis	Rose-Bengal	*t*-Amyl alcohol	R Me 90% Et 53% *cyclo*-Pr 53% *t*-Bu 54% Ph 80% *p*-ClC_6H_4 54% *p*-MeC_6H_4 63% *p*-NCC_6H_4 23%	[191]
	Juglone, pharmacological properties	Polymer-linked Rose-Bengal (Sensitox)	*t*-Amyl alcohol	57.5	[192]
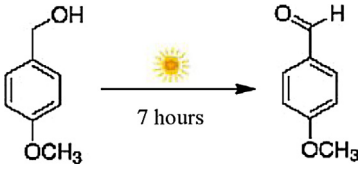	*p*-Anisaldehyde, an intermediate for pharmaceutical industry	N-doped mesoporous titania (meso-$TiO_{2-x}N_x$)	Water	25	[193]

Table 3 (*Continued*)

Photocatalytic alkylation					
Reaction	Product and use	Photocatalyst	Solvent	Yield (%)	Ref.
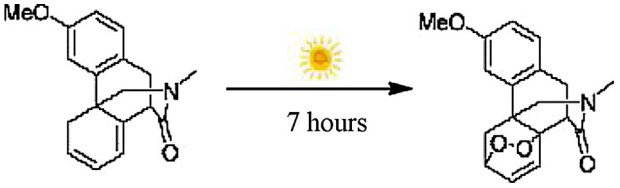	Thebaine, precursor, analgesic activity	Eosin	Ethanol	nr	[194]
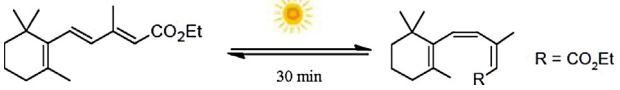	Isomer of vitamin A series	Rose-Bengal	Ethanol	30, 7-*cis* 60, 7,9-dicis	[195]
	Isomer of vitamin A series	Rose-Bengal	Ethanol	49, 7-*cis* 43, 7,9-dicis	[195]
	Isomer of vitamin A series	Rose-Bengal	Ethanol	18	[195]
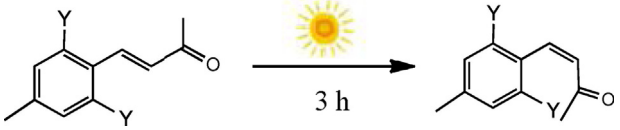	Hindered olefinic isomers	Differentsensitizers	Organic solvents	30–100	[196]
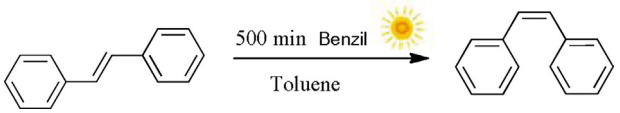	*Cis*-stilbene	Benzil	Toulene	71	[130]
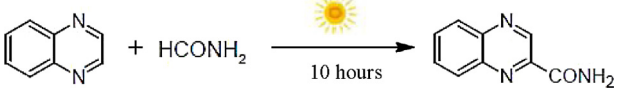	Functionalisation of some heterocyclic bases	Titania (anatase)	Formamide/sulfuric acid	100	[197]

Table 3 (*Continued*)

Photocatalytic alkylation					
Reaction	Product and use	Photocatalyst	Solvent	Yield (%)	Ref.
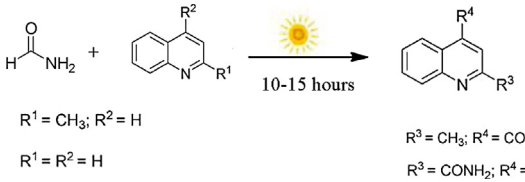	Functionalisation of some quinolines	Titania (anatase)	Formamide/sulfuric acid	90–100	[197]
	Norbornane carboxyamide	Acetone	*t*-ButOH/acetone	87	[198]
 R = R′ = CH_3; R = $CH_3(CH_2)_n$, R′ = CH_3; R = $CH_3(CH_2)_4$, R′ = CH_3; R = $CH_3(CH_2)_2$, R′ = C_2H_5 R = $CH_3(CH_2)_7$, R′ = $(CH_2)_7COOCH_3$; R = $CH_3(CH_2)_n$, R′ = $(CH_2)_7CONH_2$	Amides	Acetone	*t*-ButOH/acetone	21–51	[199]
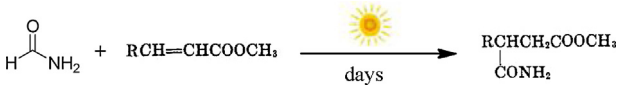	Amidoesters	Benzophenone	*t*-ButOH	80–90	[199]
	Cyclohexanecarboxamide	Acetone	*t*-ButOH/acetone	65	[199]
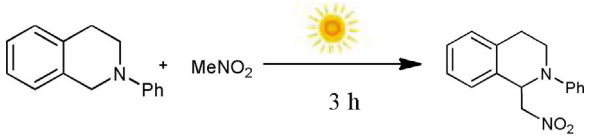	α-Functionalised tertiary amines	Rose-Bengal	Nitromethane	87	[200]

process oxidizing conditions must be avoided, and for longer equipment lifetime, any materials used must be inert to UV degradation by solar radiation [120].

The main factor affecting solar photocatalytic reactor technology costs is its scale-up. Scaling up solar photocatalytic reactors is considerably more complicated than scaling up conventional chemical reactors. In addition to conventional reactor complications, reagent and catalyst contact, flow patterns, mixing, mass transfer, and temperature control must be calculated to achieve efficient exposure of the catalyst to solar irradiation, so axial and radial scale-up are essential parameters for maximizing the surface areas exposed per unit of reactor volume, and making distribution of sunlight inside the reactor uniform. Higher illuminated surface to volume ratios reduce the reactor dimensions, and thereby, capital and operating costs.

Operating costs associated with solar concentration and its use frequently limit the potential applications of solar photocatalysis. Therefore, it is important to know how to employ solar radiation in the photoreactor efficiently, and how solar energy varies under different operating conditions. For optimum solar-assisted photocatalysis, in addition to achieving highly active photocatalysts and identifying the best operating conditions for the chemical reactions involved, special attention must also be given the photoreactor design factors that most affect use of the solar radiation.

The efficiency of the photocatalytic reactor (η) can be defined by thermodynamic principles, such as the ratio of radiant power used (Q_{used}, J s^{-1}) to radiant power absorbed ($Q_{absorbed}$) for the production of desired chemicals or for the formation of reactive species, such as hydroxyl radicals, singlet oxygen, or positive holes, which react with the chemical reagents to be converted, or adsorbed on the solid photocatalyst if a heterogeneous process is involved.

The efficiency factor η can be used as a parameter to find the energy efficiency of a solar photocatalytic reactor [121]. In heterogeneous systems, this can be expressed in terms of the specific reaction rate per unit weight of irradiated catalyst (r_s, mol g r^{-1} s^{-1}), the enthalpy of formation of the reactive species (ΔH_{rs}, J mol^{-1}) and the irradiated catalyst weight (W_{irr}, g r):

$$(eq3) \qquad \eta = \frac{Q_{used}}{Q_{absorbed}} = -\frac{V}{V_1} \times \frac{r_s \times \Delta H_{rs} \times W_{irr}}{Q_{absorbed}}$$

where ν and ν_1 are the stoichiometric coefficients of the consumption of reactive species and the substrate respectively. Thus, the basic information required for analysis of solar photocatalytic reactor efficiency is an expression containing the specific reaction rate.

The kinetics for heterogeneous photocatalytic water disinfection and heterogeneous photocatalytic abatement of a large number of organic pollutants, such as dye molecules, pesticides, herbicides and phenolic compounds or alkanes, haloalkanes, aliphatic alcohols, and carboxylic acids are extensively reported in the literature [38]. The Chick–Watson (C–W) and Hom (H) kinetic models or their empirical modifications are the most commonly used for photocatalytic water disinfection.

The C–W and H models assume that the photodisinfection rate is a function (linear in the C–W model) of the bacteria concentration and catalyst load:

$$(eq4) \qquad \ln\frac{N}{N_0} = -k \times C^n \times t^m n,\ m = 1(\text{C} - \text{W model});\ \ n, m \neq 1(\text{H model})$$

where

n, m = empirical constants,
C = photocatalyst load,
N = microorganism concentration at time t,
N_0 = initial microorganism concentration,
t = treatment time.

However, a freeware add-in Microsoft® Excel tool, named GInaFIT [Geeraerd and Van Impe Inactivation Model Fitting Tool), is now available for the describing of solar microbial photo inactivation kinetics characterized by different shapes [122,123].

The Langmuir–Hinshelwood (L–H) mechanism is usually employed to explain heterogeneous photocatalytic oxidation reactions. The L–H mechanism assumes that the photocatalytic reaction rate (r) is proportional to the fraction of the photocatalyst surface covered by the organic pollutant (θ_x):

$$(eq5) \qquad r = k_r \times \theta_x = \frac{k_r \times K \times C}{1 + K \times C}$$

where k_r is the reaction rate constant, C is the concentration of organic species, and K is the Langmuir adsorption constant. However, the reaction order in the L–H kinetic model may range from 0 to1 [41]. In fact, if the initial concentration of the organics (C_0) is low, the L–H equation can be simplified to an apparent first-order equation. For the highest concentrations C, where the KC term is much greater than one, a zero-order equation may be used. The solar photocatalytic process economics generally determine its commercial feasibility. The overall cost of a photochemical process is represented by the sum of the fixed capital, recurrent operating costs, and maintenance costs.

Since the cost of the land required for the installation of a solar photocatalytic reactor and the collector surface needed add a significant portion to the overall cost of the process, it is important to calculate the illuminated reactor area required as accurately as possible.

In this respect, the estimated price of the photochemical parabolic trough collectors (PTC) is close to \$235/m^2, for completely installed parabolic trough collectors used for solar thermal energy, and the price for the flatbed reactor is around \$200/m^2 [168].

However, the starting cost of a one sun CPC collector is estimated at around \$160/m^2. This cost includes the support structure, reflector materials, Pyrex glass tubes, labor, and manufacture. The Pyrex glass tubes are a substantial fraction of the system cost (\$51/m^2). An aluminum reflector sheet is \$10/m^2. The remaining collector costs, mainly labor, and manufacturing costs, make up about 60% of the investment [169].

A “figure of merit” can be used to assess the solar photochemical technology efficiency and related capital costs. In a solar-driven treatment system, the electrical energy component is practically absent and a solar “figure of merit” is usually defined based on the collector area necessary to achieve a specific degradation rate.

However, even though solar radiation has no cost, there could be a non-marginal capital cost for the collector. Since the capital cost of a solar collector facility is generally proportional to its land requirement, a "figure of merit" based on the solar collector area is appropriate for estimating the irradiated reactor area required [127].

For NCC, PTC, and CPC reactors, using batch or through-flow mode, the appropriate "figure of merit" are described for high and low concentrations, respectively [170].

The collector area per mass (A_{CM}, $m^2\,kg^{-1}$), defined as the collector area required to reduce a unit of substrate mass in the reactor system in a reference time of 1 h (t_0) and incident solar irradiance of 1000 $W\,m^{-2}$ ($E_s{}^0$) based on the AM1.5 standard solar spectrum on a horizontal surface, is:

$$A_{CM} = \frac{10^3 \cdot A_r \cdot t \cdot \overline{E_s}}{M \cdot V_t \cdot t_o \cdot E_S^o \cdot \left(C_i - C_f\right)} \qquad A_{CM} = \frac{10^3 \cdot A_r \cdot \overline{E_s}}{M \cdot F \cdot t_o \cdot E_S^o \cdot \left(C_i - C_f\right)}$$

(eqs6–7) "batch" "through-flow"

where A_r is the real collector area, M is the molar mass of the substrate ($g\,mol^{-1}$), V_t is the volume of treated solution (L), ($W\,m^{-2}$) is the average direct solar irradiance during reaction time t, F ($m^3\,h^{-1}$) is the flow rate, and C_i and C_f are the starting and final substrate concentrations (M), respectively. It is worth noting that the higher the A_{CM}, the lower the photoreactor efficiency is. For the natural solar TiO_2-photocatalytic production of benzaldehyde in a CPC reactor, an A_{CM} of 3.08×10^3 m^2 per kilogram and hour of benzyl alcohol converted has been reported [2].

The collector area per mass has also been used for scaling up CPC reactor parameters to find the solar collecting area required to treat different volumes of industrial wastewater using solar homogenous photocatalysis (photo-Fenton).

Depending on the type of wastewater, in this case, real wastewater, in a combined solar photocatalysis and biological treatment, the volume effluents (0.1 m^3) can be treated until the complete removal of COD using 7 m^2 of solar CPC collectors [171].

In order to include the effect of intermittent solar irradiance (E_s), the experimental data are reported as a function of the normalized illumination time (t_{30W})

$$t_{30W,n} = t_{30W,n-1} + \frac{\bar{I}_{UV,n}}{30W/m^2} \times \frac{V_i}{V_t} \times \Delta t_n;\ \ \Delta t_n = t_n - t_{n-1};\ t_0 = 0 (n = 1) \quad (eq8)$$

and accumulated energy per unit volume (Q_{jUV}):

$$Q_{jUV,n} = Q_{jUV,n} + \bar{I}_{UV,n} \times \frac{A_r}{V_t} \times \Delta t_n;\ \ \Delta t_n = t_n - t_{n-1};\ t_0 = 0 (n = 1) \quad (eq9)$$

where t_n is the experimental time of each sample, V_i the irradiated volume of solution, and the average UV irradiance (300–400 nm) during. Considering that UV irradiance is only 3.5% of all direct solar irradiance [172,173], the A_{CM} formulation is rearranged as a function of the and parameters:

$$A_{CM} = \frac{10^3 \times A_r \times 30W/m^2 \times t_{30W,f}}{M \times V_i \times t_0 \times E_s^0 \times (C_i - C_f) \times 0.035} = \frac{10^3 \times Q_{jUV,f}}{M \times t_0 \times E_s^0 \times (C_i - C_f) \times 0.035} \quad (eq10)$$

where $t_{30W,f}$ and $Q_{jUV,f}$ represent the normalized illumination time and accumulated energy per unit of volume necessary to reach concentration C_f, respectively. When the reduction in organic carbon concentration is evaluated, A_{CM} is calculated for the removal of 1 kg of organic carbon.

Several A_{CM}s have been extrapolated from the results reported in the literature for heterogeneous and homogeneous photocatalysis as examples (Tables 4 a and b).

As shown in Table 4a and b, photo-Fenton usually requires solar photoreactor surfaces smaller than those used for TiO_2 heterogeneous photocatalysis. For instance, the solar removal of imidacloprid, a neonicotinoid insecticide, by photo-Fenton in a CPC reactor is characterized by an A_{CM} of 5.54×10^2 m^2 (5a, Table 4b) and 4.58×10^3 m^2 with TiO_2 (11a, Table 4a). If the aim of the process is to mineralize pollutants, the A_{CM} values is expected to increase, since the by-products also have to be oxidized.

Another interesting example is the one reported by Bauer et al. [174], in which aqueous mixtures of 10 commercial pesticides, each at a concentration of 10 $mg\,L^{-1}$, were treated by both photo-Fenton and TiO_2 in CPC reactors to decontaminate the solution by completely oxidizing the pollutants. In this case, the A_{CM} required to totally oxidize 1 kg of organic carbon in a reference time of 1 h for 10^3 $W\,m^{-2}$ of incident solar irradiance, is 1.35×10^3 m^2 by photo-Fenton (3, Table 4b) and 1.59×10^4 m^2 by TiO_2 (10, Table 4a). These results, according to the economic evaluation reported by the authors [174], led them to the conclusion that the investment in a solar TiO_2 photocatalytic process is higher than for solar photo-Fenton due to the larger collector area required. On the other hand, the costs derived from the consumption of chemicals for a TiO_2 photocatalytic treatment are negligible compared to photo-Fenton, which requires hydrogen peroxide and mineral acids. In particular, starting hydrogen peroxide and iron concentrations not only affect chemical costs, but also reaction rates and A_{CM}. As shown in Table 4b (1a and 1b), when $FeSO_4$ and H_2O_2 are present in the solution at starting concentrations of 0.1 mM and 5.0 mM, respectively, the removal of Direct Black 38, a commercial dye, is characterized by an A_{CM} of 4.09×10^2 m^2. This decreased by 11% ($A_{CM} = 3.64 \times 10^2$ m^2) when the starting concentrations of ferrous sulfate and hydrogen peroxide were increased tenfold. Moreover, when real wastewater was treated in a CPC reactor in the presence of $FeSO_4$ and H_2O_2 at starting concentrations of 1.0 mM and 50 mM, respectively, an A_{CM} of 5.60×10^3 m^2 is required to completely oxidize 1 kg of Direct Black 38 in a reference time of 1 h at 10^3 $W\,m^{-2}$ of incident solar irradiance (Table 4b and 1c). The nearly 54% increase in A_{CM} is probably due to the presence of other substances in the real wastewater acting as hydroxyl radical scavengers [171].

To eliminate the cost of hydrogen peroxide, a modified photo-Fenton process based on oxygen as the oxidant and ferric ions as homogeneous catalysts has been proposed [175].

In this process, the sole source of hydroxyl radicals is direct photolysis of iron(III) aquo complex ($Fe(HO)^{2+}$). The catalytic cycle is closed by reoxidation of Fe^{2+} to Fe^{3+} by the dissolved oxygen. This photo-Fenton-like method was used in a CPC pilot plant at a starting Fe(III)

Table 4
"Figure of merit" A_{CM} values of heterogeneous (a) ad homogeneous (b) photocatalytic process for wastewater treatment. The grey colored fields represent values of TOC initial concentration, TOC removal and A_{CM} values calculated on the removal of 1.0 kg of total organic carbon.

Table 4a	Substance	$[C]_0$ (mg/L)	Removal (%)	V_r (L)	V_i (L)	S (m^2)	$[TiO_2]$ (mg/l)	Form	pH	Solvent	Collector geometry	A_{CM} (m^2)	Refs.
1a	Methyl-oxydemeton	50	70	25	15.1	2.15	200	Slurry (degussa P-25)	–	Water (milli Q grade)	CPC	$1.16 \times 10^{4*}$	[201]
1b	Methidathion	50	100	25	15.1	2.15	200	Slurry (degussa P-25)	–	Water (milli Q grade)	CPC	$4.06 \times 10^{3*}$	
1c	Carbaryl	50	100	25	15.1	2.15	200	Slurry (degussa P-25)	–	Water (milli Q grade)	CPC	$1.62 \times 10^{4*}$	
1d	Dimethoate	50	100	25	15.1	2.15	200	Slurry (degussa P-25)	–	Water (milli Q grade)	CPC	$8.54 \times 10^{3*}$	
2a	Progesterone	0.1	100	10	0.96	0.3	335	Immobilized (HP on glass spheres)	–	Syntetic water	CPC	$8.93 \times 10^{5*}$	[202]
2b	Triclosan	0.1	100	10	0.96	0.3	335	Immobilized (HP on glass spheres)	–	Syntetic water	CPC	$4.46 \times 10^{5*}$	
2c	Hydroxybiphenyl	0.1	100	10	0.96	0.3	336	Immobilized (HP on glass spheres)	–	Syntetic water	CPC	$2.23 \times 10^{6*}$	
2d	Diclofenac	0.1	100	10	0.96	0.3	337	Immobilized (HP on glass spheres)	–	Syntetic water	CPC	$2.23 \times 10^{6*}$	
2e	Ibuprofen	0.1	100	10	0.96	0.3	338	Immobilized (HP on glass spheres)	–	syntetic water	CPC	$2.90 \times 10^{6*}$	
2f	Ofloxacin	0.1	100	10	0.96	0.3	339	Immobilized (HP on glass spheres)	–	Syntetic water	CPC	$4.46 \times 10^{5*}$	
2g	Caffeine	0.1	100	10	0.96	0.3	340	Immobilized (HP on glass spheres)	–	Syntetic water	CPC	$1.78 \times 10^{6*}$	
2h	Acetaminophen	0.1	100	10	0.96	0.3	341	Immobilized (HP on glass spheres)	–	Syntetic water	CPC	$1.78 \times 10^{6*}$	
2i	Sulfamethoxazole	0.1	100	10	0.96	0.3	342	Immobilized (HP on glass spheres)	–	Syntetic water	CPC	$4.91 \times 10^{6*}$	
2j	Antipyrine	0.1	70	10	0.96	0.3	343	Immobilized (HP on glass spheres)	–	Syntetic water	CPC	$8.29 \times 10^{6*}$	
2k	Flumequine	0.1	100	10	0.96	0.3	344	Immobilized (HP on glass spheres)	–	Syntetic water	CPC	$1.34 \times 10^{6*}$	
2l	Isoproturon	0.1	100	10	0.96	0.3	345	Immobilized (HP on glass spheres)	–	Syntetic water	CPC	$5.35 \times 10^{6*}$	
2m	Ketorolac	0.1	100	10	0.96	0.3	346	Immobilized (HP on glass spheres)	–	Syntetic water	CPC	$5.36 \times 10^{6*}$	
2n	Carbamazepine	0.1	100	10	0.96	0.3	347	Immobilized (HP on glass spheres)	–	Syntetic water	CPC	$5.36 \times 10^{6*}$	
2o	Atrazine	0.1	80	10	0.96	0.3	335	Immobilized (HP on glass spheres)	–	Syntetic water	CPC	$7.25 \times 10^{6*}$	
3a	Cyanides	50	100	247	108	8.9	200	Slurry (100% anatase HP)	10	Desalinated water	CPC	$2.09 \times 10^{3***}$	[162]
3b	Cyanides	50	88	975	675	100	200	Slurry (100% anatase HP)	10	Raw water	CPC	$5.44 \times 10^{3***}$	
4a	2,4-Dichlorophenoxyacetic acid	28	100	247	108	8.9	200	Slurry (degussa P-25)	–	Desalinated water	CPC	$8.20 \times 10^{2*}$	[203]
5a	Oxalic acid	900	85	10	5.4	0.72	200	Slurry (>99% anatase Aldrich)	–	Water	CPC	$2.10 \times 10^{2**}$	[176]
5b	Oxalic acid	900	70	10	0.67	0.72	200	Slurry (>99% anatase Aldrich)	–	Water	PTC	$2.54 \times 10^{2**}$	
5c	Oxalic acid	900	70	10	8	0.72	200	Slurry (>99% anatase Aldrich)	–	Water	Flat tubular	$2.54 \times 10^{2**}$	
5d	Carbaryl	50.3	77	10	5.4	0.72	500	Slurry (>99% anatase Aldrich)	–	Water	CPC	$4.10 \times 10^{3**}$	
5e	Carbaryl	50.3	68	10	0.67	0.72	500	Slurry (>99% anatase Aldrich)	–	Water	PTC	$4.70 \times 10^{3**}$	
5f	Carbaryl	50.3	55	10	8	0.72	500	Slurry (>99% anatase Aldrich)	–	Water	Flat tubular	$5.92 \times 10^{3**}$	
6	Oxytetracycline	15	100	15	2.94	0.91	500	Slurry (degussa P-25)	–	Water	CPC	$8.47 \times 10^{2***}$	[204]
7	Humic acid (sodium salt)	10	90	50	16	1	20 (g/m^2)	Immolized (degussa P-25 on 1049 AHLSTROM paper)	–	Deionized water	CPC	$6.17 \times 10^{4***}$	[205]
8	Yellow cibacron FN-2R	70	95	50	16	1	20 (g/m^2)	Immolized (degussa P-25 on 1049 AHLSTROM paper)	–	Well water	FFR	$2.56 \times 10^{3***}$	[142]
9a	2,4-Dichlorophenol	8	100	15	6.5	1.4	1500	Slurry (degussa P-25)	–	Tap water	CPC	$1.20 \times 10^{4**}$	[206]
9b	2,4-Dichlorophenol	22	100	15	6.5	1.4	1500	Slurry (degussa P-25)	–	Tap water	CPC	$9.85 \times 10^{3**}$	
10	Mix 10 commercial pesticides	100	30	250	108	9	200	Slurry (degussa P-25)	–	Desalinated water	CPC	$1.59 \times 10^{4***}$	[174]
11a	Imidacloprid	52	100	40	22	3	200	Slurry (degussa P-25)	–	Desalinated water	CPC	$4.58 \times 10^{3*}$	[207]
11b		28	98									$3.19 \times 10^{4*}$	

Table 4 (*Continued*)

Table 4b	Substance	$[C]_o$ (mg/L)	Removal (%)	V_t (L)	V_i (L)	S (m^2)	[Fe] (mM)	Fe source	$[H_2O_2]$ (mM)	pH	Solvent	Collector geometry	A_{CM} (m^2)	Refs.
1a	Direct Black 38	100	80	3	0.05	0.1	0.1	$FeSO_4$	5	2	Syntetic wastewater	CPC	4.09×10^2	[171]
1b	Direct Black 38	100	90	3	0.05	0.1	1	$FeSO_4$	50 (in 2 portions)	2	Syntetic wastewater	CPC	3.64×10^2	
1c	Direct Black 38	100	60	3	0.05	0.1	1	$FeSO_4$	50 (in 2 portions)	2	Real wastewater	CPC	5.60×10^2	
2a	Phenols (from olive mill wastewaters)	3000	97	30	22.4	3.08	1	$FeSO_4$	588	2.8	Real wastewater	CPC	$5.75 \times 10^{2***}$	[159]
2b	Phenols (from olive mill wastewaters)	2800	79	30	22.4	3.08	5	$FeSO_4$	147	2.8	Real wastewater	CPC	$4.91 \times 10^{2***}$	
2c	Phenols (from olive mill wastewaters)	2700	88	19	–	1	5	$FeSO_4$	147	2.8	Real wastewater	FFR	$7.95 \times 10^{2***}$	
3	Mixture of 10 commercial pesticides	100	88	250	108	9	1	$FeSO_4$	1 (in 5 portions)	2.8	Desalinated water	CPC	$1.35 \times 10^{3***}$	[174]
4a	4-Chlorophenol	216	100	4	2	0.42	0.75	$FeSO_4$	45	2.8	Distilled water	Pool	$1.74 \times 10^{2**}$	[208]
4b	4-Chlorophenol	216	100	12	12	0.42	0.75	$FeSO_4$	45	2.8	Distilled water	Pool	75**	
4c	4-Chlorophenol	216	100	20	20	0.42	0.75	$FeSO_4$	45	2.8	Distilled water	Pool	52**	
5a	Imidacloprid	52	100	40	22	3	0.05	$FeSO_4$	15 (maintained constant)	2.8	Desalinated water	CPC	$5.54 \times 10^{2*}$	[207]
5b		28	98										$1.74 \times 10^{4*}$	
6a	Diethyl phthalate	58	100	40	22	3	0.305	$Fe(ClO_4)_3$	0	–	Desalinated water	CPC	$4.10 \times 10^{2***}$	[175]
6b		38	85										$1.36 \times 10^{3***}$	
7a	Grape juice (WG)	1185	93	40	22	3	55	$FeSO_4$	12	3	Milli-Q water	CPC	$3.89 \times 10^{2*}$	[209]
7b	Red wine (WV)	1185	46				55						8.07 × 102*	
7c	WG and WV (50:50)	1165	90				20						$1.53 \times 10^{2*}$	
7d	WG and WV (50:50)	1165	84				20						$1.64 \times 10^{2*}$	
7e	WG and WV (50:50) without ethanol	1165	96				20						$1.25 \times 10^{2*}$	

* Calculated by using the normalized illumination time (t_{30W}) necessary to reach the final conversion.

** Calculated by using the $I_{UV,n}$ during the experimental run and considering that represent only 3.5% of the global radiation.

*** Calculated by using the accumulated energy per unit of volume (Q_{jUV}) necessary to reach the final value.

concentration of 0.305 mM for the removal of diethyl phthalate (58 ppm). The A_{CM} for removal of diethyl phthalate and the corresponding TOC is 4.10×10^2 m^2 and 1.36×10^3 m^2, respectively (6a and b, Table 4b).

This A_{CM}, calculated with the data reported by Bandala et al. [176], emphasizes the importance of the reactor type chosen. In fact, as shown in 5d–f of Table 4a, under the same operating conditions, (TiO_2 load, initial pollutant concentration, and reactor irradiated surfaces), the A_{CM} changes with variations in the solar collector geometry. In particular, for CPC, PTC, and flat tubular reactors, the A_{CM} found from the experimental data for carbaryl oxidation in the presence of 500 ppm of titania (pure anatase) is 4.10×10^3 m^2, 4.70×10^3 m^2, and 5.92×10^3 m^2, respectively.

Additional results from data reported by Malato et al. [162], who described the setup of the first industrial European solar detoxification plant, a 100 m^2 CPC designed for the batch treatment of at least 2 m^3 of water and aerated aqueous suspensions of polycrystalline TiO_2. Plant performance was compared to smaller CPC pilot plants at the Plataforma Solar de Almeria using cyanide at a starting concentration of 50 ppm as the model compound and 200 ppm of in-house prepared anatase catalyst. A_{CM} calculated from the data of the two experimental runs was 2.09×10^3 m^2 and 5.44×10^3 m^2 for the pilot and industrial treatment plant, respectively (3a and b, Table 4a). The A_{CM} in the larger plant was over 150% higher for two reasons: the O_2 concentration dropped, becoming limiting, and the experimental runs in the industrial plant were carried out with raw water which is rich in inorganic anions able to react with HO radicals and photo-generated holes [177].

Table 5 shows the A_{CM} for photocatalytic production of fine chemicals. Like the results above, it is observed that homogeneous photocatalytic processes are characterized by a lower A_{CM} than TiO_2 photocatalysis. In particular, in presence of Rose-Bengal and isopropanol alcohol, or benzophenone disodium disulfonate (BPSS), the A_{CM} is less than 4.00×10^2 m^2 in all cases studied (Table 5, 1–9). On the other hand, if TiO_2 as pure anatase and cupric ions are used to produce benzaldehyde by selectively oxidizing the benzyl alcohol, the A_{CM} is lowered to 3.19×10^3 m^2 (Table 5, 10), which could be considered low compared to those shown in Table 4a with TiO_2 photocatalysis.

The "figure of merit" for photocatalytic disinfection is the collector area required to decrease the starting microorganism concentration 6-log in a reference time of 1 h (t_0) with incident solar irradiance of 1000 W m^{-2} ($E_s{}^0$):

$$(eq11) \qquad A_{CX} = \frac{6 \times A_r \times t \times \overline{E}_s}{t_0 \times E_s^0 \times (\log X_i - \log X_f)}$$

where A_r is the real collector area, (W m^{-2}) is the average direct solar irradiance during reaction time t, and X_i, and X_f are the starting and final microorganism concentrations (CFU/100 mL or MPN/mL), respectively.

A_{CX} could also be calculated as a function of the final Q_{jUV} or $t_{30\,W}$:

$$(eq12) \qquad A_{CX} = \frac{6 \times Q_{jUV,f} \times V_t}{t_0 \times E_s^0 \times (\log X_i - \log X_f) \times 0.035} = \frac{6 \times A_r \times t_{30W,f} \times 30 \mathrm{W/m^2}}{t_0 \times E_s^0 \times (\log X_i - \log X_f) \times 0.035}$$

where V_t is the total solution volume. The term 0.035 refers to the fact that UV radiation between 300 m and 400 nm is only 3.5% of the daily global solar radiation.

The use of a figure of merit (A_{CM}) to estimate the surface area required to decontaminate a certain volume of polluted water is based on the concept that the more photons received in the system, the more oxidation there is on the organic molecules. However, in disinfection, the mechanism is not exactly the same. While it is true that the more radiation a system receives, the stronger the bactericidal effect, the bactericidal damage depends strongly on how the radiation is delivered to the system. If the radiation is continuous and uninterrupted during treatment, then the germicidal effect is much more effective than intermittent delivery of the same amount of energy to the same water [210]. Irradiance (i.e., solar intensity in terms of W m^{-2}) also plays an important role. For example, the log decrease in bacteria observed for the same dose (total energy) received by the system at low irradiance is different from the decrease observed at higher irradiance [211].

This can be attributed to bacterial defense mechanisms which develop under stress, like UVA irradiation or hydroxyl radicals. If the bacteria are under UVA stress, but are not killed effectively during the exposure time, then they respond to that stress with these defense mechanisms and become resistant to treatment. This is why, due to dark regions in the reactor, recirculated flow reactors are not always as effective as stationary batch reactors for disinfection. Therefore, sequential batch reactors [212] and others [213] have been designed to achieve higher effective disinfection efficiency under outdoor conditions.

The per order collector area (A_{CO}, m^2 m^{-3} order^{-1}) is the collector area needed to reduce substrate concentration by one order of magnitude per unit of volume (e.g., 1 m^3) in water or air with "standardized" incident solar irradiance ($E_s{}^0$) of 1000 W m^{-2} (AM1.5 standard solar spectrum) on a horizontal surface over a reference period of 1 h (t_0):

$$A_{CO} = \frac{A_r \cdot t \cdot \overline{E_s}}{V_t \cdot t_o \cdot E_S^o \cdot log\left(\frac{C_i}{C_f}\right)} \qquad \text{"batch"}$$

$$A_{CO} = \frac{A_r \cdot \overline{E_s}}{F \cdot t_o \cdot E_S^o \cdot log\left(\frac{C_i}{C_f}\right)} \qquad \text{"flow"}$$

(eqs13–14)

"Figures of merit" enable system costs to be estimated quickly and provide an indication of the capital investment required for solar photocatalytic NCC, CPC, or PPC reactors, although there may be other cost factors, like chemicals and operation/maintenance, which would have to be included in a complete cost analysis.

The operating costs can be calculated by the sum of the costs of each liquid chemical (X_i) and solid (Y_j) reagents, assuming the cost of energy associated with a solar process to be zero [214]:

$$\text{Operating costs} = \sum_{i=1}^{n} cost_{X_i} + \sum_{j=1}^{m} cost_{Y_j} \quad \text{with} \quad cost_{X_i} = \frac{\text{price}X_i(€/\text{ton}) \times C_{X_i} 10^{-3}(\text{ton/m}^3) \times \rho_{X_i}(\text{kg/L})}{\%\text{of purity}/100(\text{kg/L})}$$

for liquid reagents and

$$cost_{Y_j} = \frac{\text{price}Y_j(€/\text{ton}) \times C_{Y_j} \times 10^{-6}(\text{ton/m}^3) \times \text{MW}_{\text{starting material}}/\text{MW}_{Y_j}}{\%\text{of purity}/100}$$

for solid reagents.

Table 5
"Figure of merit" A_{CM} values of photocatalytic process aimed at the production of fine chemicals.

	Reagent	Product	$[C]_0$ (mg/L)	Conversion (%)	Selectivity (%)	V_r (L)	V_i (L)	S (m^2)	Solvent	Catalyst/sensitizer	[Catalyst] (mg/L)	Collector geometry	A_{CM} (m^2)	Refs.
1	Citronellol	Rose Oxide	85000	100	55	80	–	32	Isopropanol	Rose-Bengal	450	PTC	9	[131]
2	1,5-Dihydroxynaphthalene	Juglone	5000	100	80	0.2	–	0.188	Isopropanol	Rose-Bengal	500	PTC	2.35×10^2	
4	Maleic acid Isopronanol	Terebic acid	11607 Large excess	90	83	1.2	–	0.2	Isopropanol-water (1:1)	BPSS	3858	CPC	$1.23 \times 10^{2*}$	[165]
5	Acetylenedicarboxylic acid Isopronanol	Bis(γ-methyl)-di-valerolactone	7984 Large excess	35	43	1.2	–	0.2	Isopropanol-water (1:1)	BPSS	3858	CPC	$1.49 \times 10^{2*}$	
6	*trans*-2-Hexenal Isopropanol	β-propyl-γ-di-methyl-valerolactol	9814 Large excess	83	66	1.2	–	0.2	Isopropanol-water (1:1)	BPSS	7716	CPC	97*	
7	Crotonaldehyde Isopropanol	β,γ,γ'-tri-methyl-valerolactol	7000 Large excess	55	55	1.2	–	0.2	Isopropanol-water (1:1)	BPSS	3858	CPC	$3.76 \times 10^{2*}$	
8	Crotonaldehyde 1,3-Dioxolane	1,3-Dioxolane-2-(3-butyraldehyde)	7000 Large excess	80	31	1.2	–	0.2	1,3-Dioxolane-water (5:7)	BPSS	3858	CPC	$2.11 \times 10^{2*}$	
9	*trans*-2-Hexenal 1,3-Dioxolane	1,3-Dioxolane-2-(3-capronaldehyde)	9814 Large excess	88	40	1.2	–	0.2	1,3-Dioxolane-water (5:7)	BPSS	7716	CPC	91*	
10	Benzyl alcohol	Benzaldehyde	162	62	70	39	22	3	Desalinated water	TiO_2 (Aldrich pure anatase) Cu (added as $CuSO_4$)	200 63.5	CPC	3.19×10^3	[2]

* Calculated by using the $\bar{I}_{UV,n}$ during the experimental run and considering that represent only 3.5% of the global radiation.

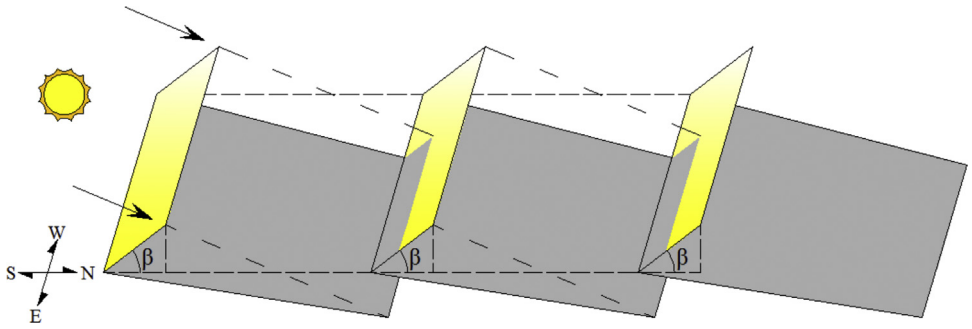

Fig. 13. Shading by collectors in a solar field.

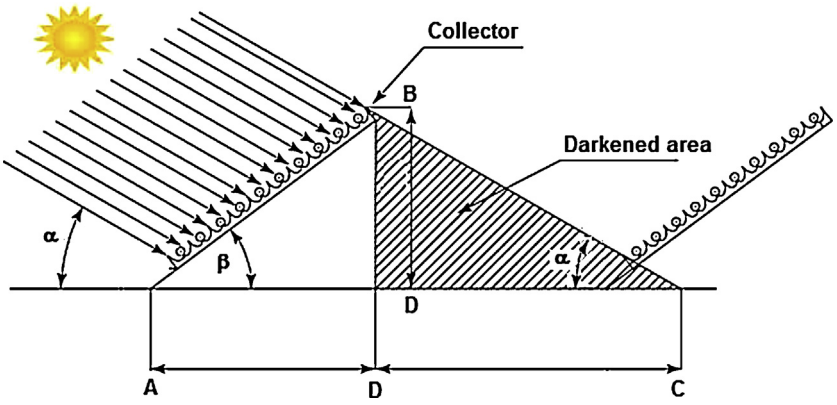

Fig. 14. Estimation of the minimum distance between the rows to minimize the shadowing the collectors.

Once A_{CM} has been estimated, particularly if many mirrors are required in a limited field, the optimal design of the solar field should minimize plant costs and avoid shading and masking effects that decrease the incident solar energy on the collectors (Fig. 13) [215].

In this regard, the dark area can be estimated by calculating the shortest distance ($\overline{AC}$) between the rows to minimize collector shadowing.

Defining as the solar altitude angle (Fig. 14), that is the angle between the solar rays and the horizontal terrestrial plane at a given latitude, as the collector inclination, which should be equal to the local latitude, and as the collector height (known from A_{CM}), the segment may be estimated by calculating angles AC, AD and DC, respectively:

$$(eq15) \qquad A\hat{B}C = 180^\circ - \alpha - \beta,\ A\hat{B}D = 90^\circ - \beta,\ D\hat{B}C = A\hat{B}C - A\hat{B}D = 90^\circ - \alpha$$

It is trigonometric fact that:

$$(eq16) \qquad \overline{BD} = \overline{AB} \times \sin\beta,\ \overline{AD} = \overline{AB} \times \cos\beta,\ \overline{DC} = \overline{BD} \times \tan D\hat{B}C = \overline{AB} \times \sin\beta \times \tan(90^\circ - \alpha)$$

From the above formulas, the distance between two collectors is:

$$(eq17) \qquad \overline{AC} = \overline{AD} + \overline{DC} = \overline{AB} \times [\cos\beta + \sin\beta \times \tan(90^\circ - \alpha)]$$

5. Factors affecting solar photocatalysis

5.1. Solar irradiance and weather conditions

As expected, solar photocatalytic reaction rates increase with increasing solar irradiance which is indirectly related to the quantum yield of the overall process (Q_y). In fact, the total number of photons received by a photoreactor can be calculated by measuring and integrating the solar irradiance around the reactor walls. Obviously, under uncontrollable weather conditions and low solar intensities (overcast and rainy days), the quantum yield dependence on irradiance cannot be calculated. In heterogeneous photocatalysis, reaction rate profiles are proportional to the number of incoming photons on the solid photocatalyst (Fig. 15).

Performance is almost linear when solar irradiance is low. Above a certain amount, depending on reaction conditions (photocatalyst, target compounds, photoreactor design, etc.), the reaction rate becomes proportional to the square of the solar irradiance. At very high solar irradiances, the reaction rates become independent of radiation intensity.

Some studies have reported that the reason for the square root relationship is explained by bulk recombination of photoelectron-hole pairs within the catalyst particles [216,217]. Furthermore, at sufficiently high light intensity, the photocatalytic reaction is no longer dependent on radiation received, and depends only on mass transfer within the reaction. So the rate remains constant even though radiation increases. This effect can appear for different reasons, such as lack of electron scavengers (i.e., O_2), or organic molecules in the proximity of TiO_2 surfaces, and/or excess of products occupying active catalyst centers, etc. These phenomena appear more frequently when working with supported catalysts, and/or with slow agitation, implying less catalyst surface in contact with the liquid and less turbulence. This does not favor the contact of reactants with the catalyst.

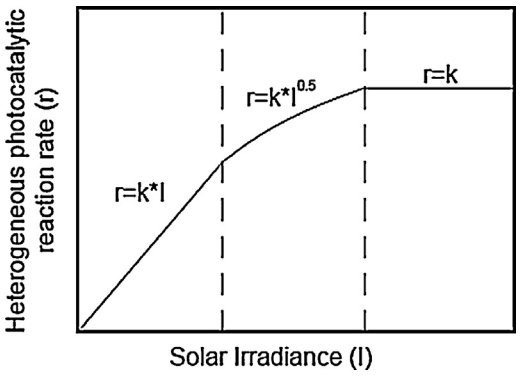

Fig. 15. Heterogeneous photocatalytic reaction rate vs solar irradiance.

This result, and the need for cooling units necessary for solar photoreactors which employ sunlight concentrators, led research to gradually focus on CPC systems instead of PTCs for solar photocatalytic applications.

5.2. Catalyst load, optical density, photoreactor diameter, and specific area

Catalyst load, or in homogeneous processes, its concentration, system optical density, and solar photoreactor diameter are essential, mutually interrelated reactor design parameters. With photocatalytic heterogeneous slurries, both light absorption and scattering by catalyst particles must be taken into account for optimal reactor light-path length and catalyst loads.

In fact, in heterogeneous slurries, the reaction rate increases with increasing catalyst load, but decreases over a certain amount [218,219]. At the highest particle concentrations, photocatalytic activity falls, mainly because sunlight is scattered, particles agglomerate, and photon flux penetration in the mixture is poor. Therefore, in slurry reactors, the photocatalyst load must be optimized for best photocatalytic activity [220,221]. Larger photoreactor diameters result in a lower optimum catalyst load, and vice versa [222]. From a practical point of view, the ideal diameter of the solar photoreactor must be in the 25–50 mm range [140,223,224]. Less than 20–25 mm diameters are not feasible, because of operating pressure loss. In photocatalytic reactors employing immobilized photocatalyst particles, the film thickness is crucial. The incoming solar photons are only partly absorbed when films are very thin (<1 m), whereas, thick catalyst films cause an unreactive “dark zone” directly below the catalytic surface exposed. The optimal photocatalyst film depends on several parameters, such as the solar wavelength range, the physical and optical characteristics of the material used and the photocatalyst deposition technique [225,226].

In heterogeneous reactions, the specific surface area is another key factor, since it is proportional to the density of active catalytic sites. It has been demonstrated that the activity of a heterogeneous photocatalyst is not simply correlated with its specific surface area, but is controlled by photoinduced electron transfer [227–229]. However, the specific surface areas for the most commonly used photocatalysts are listed in Table 6. Like heterogeneous photocatalysis, in homogeneous photocatalysis, the catalyst concentration is affected by the light-path length. For photo-Fenton, it has been demonstrated that the optimum ferric ion concentration is about 0.2–0.5 mM, regardless of photoreactor type [151,230].

5.3. Oxygen concentration

Dissolved oxygen concentration has a fundamental role in photocatalytic reactions, since it reacts with photogenerated electrons forming radical oxidizing species and helping prevent very fast recombination of photoelectrons and holes [231,232]. There is a consensus in the literature regarding the influence of oxygen. Oxygen is necessary for complete mineralization and does not seem to be competitive with other reagents during adsorption on TiO_2, since oxidation takes place at a different location from reduction. The concentration of oxygen also affects the reaction rate, but it seems that the difference between air (P_{O_2} = 0.21 atm) and pure oxygen (P_{O_2} = 1 atm) is not very great. In an industrial plant it would simply be a matter of economy of design. It has been reported that the rate of oxidation is independent of oxygen concentration up to air saturation, suggesting that mass transfer of oxygen to the surface could also be rate limiting.

5.4. Effect of original pH

The pH of the solution affects both heterogeneous and homogeneous solar photocatalysis. Heterogeneous photocatalysts generally show a strong pH dependency of the surface charge state and the band gap potential. According to Nerst’s law, when the solution pH is varied, the valence energy and conduction band edges shift by 0.059 per unit pH at room temperature [42]. This makes the valence band electron more effective, and the conduction band holes less effective at higher pH.

Additionally, if the surface of catalyst is characterized by amphoteric groups, such as titania, then:

$$(r18) \qquad MOH + H^+ \overset{pK_{a1}}{\rightleftharpoons} MOH_2^+$$

$$(r19) \qquad MOH + HO^\bullet \overset{pK_{a2}}{\rightleftharpoons} MO^- + H_2O$$

where MOH, MOH_2^+, and MO^- are the neutral, positive, and negative surface hydroxyl groups, respectively. The point of zero charge (pH_{zpc}) can be calculated as:

$$pH_{zpc} = \frac{1}{2}(pK_{a1} + pK_{a2})$$

Table 6
pH_{zpc} and BET specific surface areas for the more common used photocatalysts.

	pH_{zpc}	BET (m^2/g)
TiO_2		
Degussa P25 (Evonik) ~80% anatase, ~20% rutile	6.3[a]	50.0[a]
Anatase 100% (Aldrich)	4.2[a]	9.2[a]
Anatase 100% nanopowder (Aldrich)	5.2[b]	335.0[e]
Rutile 100% (Aldrich)	4.8[a]	1.9[a]
Rutile 100% (Tioxide Specialities Ltd., UK)	5.4[c]	17[c]
Rutile P25	6.1[a]	29.2[a]
Millenium PC100 (Millenium Inorganic Chemicals)	5.9[a]	89.6[a]
Millenium PC500 (Millenium Inorganic Chemicals)	6.2[a]	287.0[a]
Hombikat UV 100 (Sachtleben chemie GmbH)	6.0[a]	348.0[a]
TiO_2 (Junsei)	4.4[a]	9.7[a]
TiO_2 ST-01 (Ishihara)	5.8[a]	340.0[a]
Combustion synthesized TiO_2	2.4[d]	246[d]
ZnO		
ZnO (Aldrich)	9.2[b]	
ZnO (Bio-Tech)	8.0[g]	
Fe_2O_3		
Fe_2O_3 (Aldrich)	6.5[b]	
Fe_2O_3 (Home prepared)	8.4[b]	
Fe_2O_3 (Home prepared)	9.5[f]	

[a] [227].
[b] [238].
[c] [239].
[d] [240].
[e] [241].
[f] [242].
[g] [243].

where pK_{a1} and pK_{a2} are the negative logarithms of dissociation constants in acid and alkaline media, respectively.

When the $pH < pH_{zpc}$, the surface charge of the catalyst is positive, if $pH > pH_{zpc}$ it is negative, and it is neutral when $pH = pH_{zpc}$.

These characteristics significantly affect the adsorption–desorption properties of the photocatalyst surface [233]. For example, for Degussa P-25 (Evonik) TiO_2, the most widely used titania for photocatalytic processes in aqueous media, pH_{zpc} is from 6.25 to 6.60 [234]. As a reference organic compound, phenol, which has a pK_a of 9.95, can be charged positively or negatively depending on the pH range, and consequently, interaction with Degussa P-25 titania changes with the pH of the solution. In acidic media, phenol is mainly present in its nonionic form, and its adsorption on the positively charged catalyst surface is noticeably promoted, and therefore, the photocatalytic oxidation rate is enhanced. On the other hand, in alkaline media, phenol exists primarily as phenolate anions and the Degussa P-25 TiO_2 surface is negatively charged. Thus, Coulombic repulsion between the negatively charged photocatalyst particle surface and phenolates could prevent its adsorption and the reaction rate would be slowed down [235]. The pH_{zpc} also changes significantly with the synthesis techniques, the type of photocatalyst [227,236], structural and adsorbed impurities and textural defects (Table 6) [237].

However, the effect of pH on heterogeneous photocatalysis is almost controversial, since the positive holes are considered the major oxidation species at low pH whereas, hydroxyl radicals are considered the predominant species at neutral or high pH [244,245].

Moreover, it should be kept in mind that pH_{zpc} is measured on unirradiated catalyst samples, and therefore, it may not always be correct to extrapolate those measurements to illuminated conditions. For example, tests performed on illuminated heterogeneous photocatalysts have demonstrated that the equilibrium adsorption constants of organics on these solids are generally higher than those measured separately under dark conditions [246], confirming that the distribution of amphiphilic and hydrophobic surface sites for a same photocatalyst changes depending on lighting conditions.

One very important feature of photocatalysis often not taken into consideration for decontamination of water is that during the reaction, a multitude of intermediate products are produced that may behave differently depending on the pH of the solution. Consideration of only the original substrate decomposition rate could lead to taking an erroneous pH as the best for contaminant degradation. Therefore, a detailed analysis of pH should include not only the initial substrate, but also the rest of the compounds produced during the process. Measurement of an overall parameter, such as TOC (or COD, or toxicity, or biodegradability, etc.) should be used for choosing the optimum pH, or at least to determine the effect of pH on behavior of the key parameter chosen.

Homogeneous photocatalytic reactions are usually strongly pH-dependent. For example, in the photo-Fenton treatments, pollutant degradation rates decrease at pH over 3.5 due to the precipitation of iron as hydroxide [247]. Moreover, it is known that the oxidation potential of hydroxyl radicals generated during the photocatalytic process decreases with increasing pH [248]. Finally, a further reason for less efficient degradation at pH over 3.5 is attributed to the dissociation and auto-decomposition of the hydrogen peroxide used as a reagent in photo-Fenton systems [249].

When pH is too acid (below 2.0), $HO^{\bullet}$ production is strongly affected by hydroxyl-radical scavenging by proton ions [248]. The formation of oxonium ions ($H_3O_2^+$) enhances the stability of H_2O_2 and reduces hydroxyl radical generation [250].

5.5. Effect of temperature

Homogeneous photocatalysis kinetic rate constants (i.e., photo-Fenton) are significantly affected by reaction temperature [251], and increase with increasing temperature up to a limit, above which reactions rates fall due to thermal decomposition and/or significant loss

of iron by precipitation [252]. However, for the photo-Fenton process the effect of the reaction temperature caused by the Fenton thermal reaction can be important on the reactor performance [116].

In heterogeneous systems, the band-gap energy of the photocatalyst is too high (3.0 eV for TiO_2) to be affected by thermal activation energy (kT = 0.026 eV at 25 °C for TiO_2) so heterogeneous photocatalysis is not usually very temperature-sensitive, and very little information is available concerning the influence of temperature on it [253].

A temperature increase usually promotes electron-hole recombination [254] and speeds up diffusion of hydroxyl radicals from the surface of the solid photocatalyst to the bulk liquid.

However, when temperatures are too high, the adsorption capacity of solid substrates is reduced, oxygen is dissolved, and as adsorption is a spontaneous exothermic phenomenon, superficial reaction rates of other reagents decrease [255,256].

Moreover, a negative effect of temperature on the concentration of dissolved oxygen in the bulk liquid may be expected, in the sense that if it is too low, it may allow photoelectron-hole recombination.

6. Conclusions

At the International Congress of Applied Chemistry held in New York in 1912, Ciamician presented his remarkable vision of "The Photochemistry of the Future" [257]. On that occasion, he outlined his belief that photochemistry, which was an entirely solar discipline at that time, could be an essential component of industry in the future: "*On the arid lands there will spring up industrial colonies without smoke and without smokestacks; forests of glass tubes will extend over the plains, and glass buildings will rise everywhere; inside of these will take place the photochemical processes that hitherto have been the guarded secret of the plants, but that will have been mastered by human industry which will know how to make them even more abundant fruit than nature, for nature is not in a hurry and mankind is*".

Ciamician's dream has not yet been realized. Although solar photocatalysis has produced significant interest in research, it is still too young for commercialization: there are only a few examples of medium and large-scale solar photocatalytic chemical processes in industry.

However, these few demonstrate that solar photochemical production of selected fine chemicals and solar photocatalytic wastewater treatment, particularly in sunnier regions, may be environmentally-friendly alternatives to existing conventional processes.

The results found from solar photocatalytic technologies employed in different markets encourage further research in the use of solar photochemistry to advance in the field of commercial and industrial processes.

In particular, application of heterogeneous solar photocatalysis with TiO_2 should have a future beneficial impact on the environment, public health and a greener economy, and thereby, on the quality of life.

In any case, some barriers still need to be overcome:

- Solar chemical processes require photoreactors specifically designed for a light source.
- During scale-up, it is very difficult to reproduce the same ratio of irradiated surface to total volume.
- Photochemical processes are usually characterized by a "quantum yield" of less than one, making the use of more efficient catalytic systems necessary.
- Individualization of solar-specific reactions and optimization of operating conditions, in particular, the solar radiation-catalyst interaction.
- Lack of "in situ" experiments on the long-term reliability of solar operation.
- Suppression of charge recombination in photosemiconductor materials still needs to be addressed.

If the photochemical approach can overcome certain drawbacks of conventional operations, the industrial acceptance of solar photocatalytic reactions will increase considerably.

Acknowledgments

The Authors would like to thank the anonymous reviewers for their valuable comments and suggestions to improve the quality of the paper.

References

[1] I. Dincer, Renew. Sustain. Energy Rev. 4 (2000) 157–175.
[2] D. Spasiano, L.P. Rodriguez, J.C. Olleros, S. Malato, R. Marotta, R. Andreozzi, Appl. Catal. B: Environ. 136–137 (2013) 56–63.
[3] Y. Ohama, D. Van Gemert, Application of Titanium Dioxide Photocatalysis to Construction Materials: State-of-the-Art Report of The RILEM Technical Committee 194-TDP, Springer, New York, 2011.
[4] D. Jing, L. Guo, L. Zhao, X. Zhang, H. Liu, M. Li, S. Shen, G. Liu, X. Hu, X. Zhang, K. Zhang, L. Ma, P. Guo, Int. J. Hydrogen Energy 35 (2010) 7087–7097.
[5] S. Malato, P. Fernandez-Ibanez, M.I. Maldonado, J. Blanco, W. Gernjak, Catal. Today 147 (2009) 1–59.
[6] K. Hashimoto, H. Irie, A. Fujishima, Jpn. J. Appl. Phys. 44 (2005) 8269–8285.
[7] D.W. Banhemann, Solar Energy 77 (2004) 445–459.
[8] A. Mills, S.K. Lee, J. Photochem. Photobiol. A: Chem. 152 (2002) 233–247.
[9] M.M. Gagliardi, Photocatalysts: Technologies and Global Market, BCC Research Report, March, 2010.
[10] BCC Research Market Research Reports and Technical Publications, Product Catalog, December 2012, http://www.bccresearch.com
[11] H. Tong, S. Ouyang, Y. Bi, N. Umezawa, M. Oshikiri, J. Ye, Adv. Mater. 24 (2012) 229–251.
[12] X. Chen, S.S. Mao, Chem. Rev. 107 (2007) 2891–2959.
[13] H.D. Roth, Angew. Chem. 28 (1989) 1193–1207.
[14] G.O. Schenck, K. Ziegler, Naturwissenschaften 32 (1944) 157–161.
[15] G.O. Schenck, Angew. Chem. 64 (1952) 12–23.
[16] A.M. Braun, M.T. Maurette, E. Oliveros, Photochemical Technology, Wiley, West Sussex, England, 1991.
[17] A. Fujishima, K. Honda, Nature 238 (1972) 37–38.
[18] S. Malato, J. Blanco, A. Vidal, C. Richter, Appl. Catal. B: Environ. 37 (2002) 1–15.
[19] R. Goslich, R. Dillert, D. Bahnemann, Water Sci. Technol. 36 (1997) 137–148.
[20] K. Pacheco, A.S. Watt, C.S. Turchi, In: A. Kirkpatrick, W. Worek (Eds.), ASME/ASES Joint Solar Energy Conference, 1993, pp. 43–49.
[21] D.J. Alpert, J.L. Sprung, J.E. Pacheco, M.R. Prairie, H.E. Reilly, T.A. Milne, M.R. Nimlos, Solar Energy Mater. 24 (1991) 594–607.
[22] B.P. Gupta, J.V. Anderson, Solar Energy Mater. 24 (1991) 40–61.

[23] J.E. Pacheco, M. Prairie, L. Evans, L. Yellowhorse, Proceedings 25th Intersociety Energy Conversion Engineering Conference, Reno, Nevada, 1990, pp. 141–145.
[24] C. Minero, E. Pelizzetti, S. Malato, J. Blanco, Chemosphere 26 (1993) 2103–2119.
[25] S.E. Braslavsky, A.M. Braun, A.E. Cassano, A.V. Emeline, M.I. Litter, L. Palmisano, V.N. Parmon, N. Serpone, Pure Appl. Chem. 83 (2011) 931–1014.
[26] M. Rodriguez, S. Malato, C. Pulgarin, S. Contreras, D. Curco, J. Gimenez, S. Esplugas, Solar Energy 79 (2005) 360–368.
[27] R. Andreozzi, M. Canterino, R. Marotta, Water Res. 40 (2006) 3785–3792.
[28] S.H. Bossmann, E. Oliveros, S. Göb, S. Siegwart, E.P. Dahlen, L. Payawan Jr., M. Straub, M. Wörner, A.M. Braun, J. Phys. Chem. A 102 (1998) 5542–5550.
[29] O. Legrini, E. Oliveros, A.M. Braun, Chem. Rev. 93 (1993) 671–698.
[30] F.J. Rivas, F.J. Beltrán, J. Frades, P. Buxeda, Water Res. 35 (2001) 387–396.
[31] J.J. Pignatello, E. Oliveros, A. MacKay, Environ. Sci. Technol. 36 (2006) 1–84.
[32] F. Torrades, M. Pérez, H.D. Mansilla, J. Peral, Chemosphere 53 (2003) 1211–1220.
[33] J.D. Spikes, in: K.C. Smith (Ed.), The Science of Photobiology, Plenum Press, New York and London, 1989, pp. 79–110.
[34] M. Canterino, I. Di Somma, R. Marotta, R. Andreozzi, V. Caprio, J. Photochem. Photobiol. A: Chem. 210 (2010) 69–76.
[35] M.C. De Rosa, R.J. Crutchley, Coord. Chem. Rev. 233–234 (2002) 351–371.
[36] D. Faust, K.H. Funken, G. Horneck, B. Milow, J. Ortner, M. Sattlegger, M. Schäfer, C. Schmitz, Solar Energy 65 (1999) 71–74.
[37] M. Mrowetz, W. Balcerski, A.J. Colussi, M.R. Hoffmann, J. Phys. Chem. B 108 (2004) 17269–17273.
[38] M.N. Chong, B. Jin, C.W.K. Chow, C. Saint, Water Res. 44 (2010) 2997–3027.
[39] K. Rajeshwar, M.E. Osugi, W. Chanmanee, C.R. Chenthamarakshan, M.V.B. Zanoni, P. Kajitvichyanukul, R. Krishnan-Ayer, J. Photochem. Photobiol. C: Photochem. Rev. 9 (2008) 171–192.
[40] M. Kitano, M. Matsuoka, M. Ueshima, M. Anpo, Appl. Catal. A: Gen. 325 (2007) 1–14.
[41] O. Carp, C.L. Huisman, A. Relle, Prog. Solid State Chem. 32 (2004) 33–177.
[42] M.R. Hoffmann, S.T. Martin, W. Choi, D.W. Bahnemann, Chem. Rev. 95 (1995) 69–96.
[43] A.L. Linsebigler, G. Lu, J.T. Yates, Chem. Rev. 95 (1995) 735–758.
[44] M.A. Fox, M.T. Dulay, Chem. Rev. 93 (1993) 341–350.
[45] U.I. Gaya, A.H. Abdullah, J. Photochem. Photobiol. C: Photochem. Rev. 9 (2008) 1–12.
[46] M. Ni, M.K.H. Leung, D.Y.C. Leung, K. Sumathy, Renew. Sustain. Energy Rev. 11 (2007) 401–425.
[47] K. Demeestere, J. Dewulf, H. Van Langenhove, Crit. Rev. Environ. Sci. Technol. 37 (2007) 489–538.
[48] M. Matsuoka, M. Kitano, M. Takeuchi, K. Tsujimaru, M. Anpo, J.M. Thomas, Catal. Today 122 (2007) 51–61.
[49] R. Vinu, D.G. Madras, J. Indian Inst. Sci. 90 (2010) 189–230.
[50] A. Fujishima, K. Hashimoto, T. Watanabe, TiO_2 Photocatalysis: Fundamentals and Applications, BKC Inc., Tokyo, 1999.
[51] D. Li, H. Huang, X. Chen, Z. Chen, W. Li, D. Ye, X. Fu, J. Solid State Chem. 180 (2007) 2630–2634.
[52] V. Augugliaro, M. Litter, L. Palmisano, J. Soria, J. Photochem. Photobiol. C: Photochem. Rev. 7 (2007) 123–144.
[53] A.O. Ibhadon, P. Fitzpatrick, Catalysts 3 (2013) 189–218.
[54] K. Cendrowski, X. Chen, B. Zielinska, R.J. Kalenczuk, M.H. Rummeli, B. Buchner, R. Klingeler, E. Borowiak-Palen, J. Nanopart. Res. 13 (2011) 5899–5908.
[55] M.A. Lazar, S. Varghese, S.S. Nair, Catalysts 2 (2012) 572–601.
[56] D.W. Banhemann, Res. Chem. Intermed. 26 (2000) 207–220.
[57] H. Ibrahim, H. De Lasa, Chem. Eng. Sci. 58 (2003) 943–949.
[58] R. Wang, K. Hashimoto, A. Fujishima, M. Chikuni, E. Kojima, A. Kitamura, M. Shimohigoshi, T. Watanabe, Adv. Mater. 10 (1998) 135–138.
[59] K.H. Funken, F.J. Muller, J. Ortner, K. Jurgen, R.C. Sattler, Energy 24 (1999) 681–687.
[60] J. Chen, C. Poon, Build. Environ. 44 (2009) 1899–1906.
[61] A. Fujishima, T.N. Rao, D.A. Tryk, J. Photochem. Photobiol. C: Photochem. Rev. 1 (2000) 1–21.
[62] A. Fujishima, X. Zhang, D.A. Tryk, Surf. Sci. Rep. 63 (2008) 515–582.
[63] M. Stamate, G. Lazar, Rom. Technol. Sci. Acad. 3 (2007) 280–285.
[64] X. Zhao, Q. Zhao, J. Yu, B. Liu, J. Non-Cryst. Solilds 354 (2008) 1424–1430.
[65] A. Mills, A. Lepre, N. Elliot, S. Bhopal, I.P. Parkin, S.A. O'Neill, J. Photochem. Photobiol. A: Chem. 160 (2003) 213–224.
[66] I.P. Parkin, R.G. Palgrave, J. Mater. Chem. 15 (2005) 1689–1695.
[67] A. Fujishima, X.T. Zhang, C.R. Chim. 9 (2006) 750–760.
[68] C.L. Bai, Science 309 (2005) 61–63.
[69] A.M. Ramirez, K. Demeestere, N. De Belie, T. Mantyla, E. Levanen, Build. Environ. 45 (2010) 832–838.
[70] S. Guo, Z.B. Wu, W.R. Zhao, Chin. Sci. Bull. 54 (2009) 1137–1142.
[71] E. Puzenat, Eur. Phys. J. Conf. 1 (2009) 69–74.
[72] L. Cassar, C. Pepe, G. Tognon, G.L. Guerrini, R. Amadelli, Proceeding 11th International Congress on the Chemistry of Cement. The Cement and Concrete Institute of South Africa, Durban, 2003, pp. 2012–2021.
[73] G.L. Guerrini, A. Plassais, C. Pepe, L. Cassar, in: L. Cassar, P. Baglioni (Eds.), Proceedings of Int. RILEM Symposium on Photocatalysis 'Environment and Construction Materials, Florence, Italy, 2007, pp. 219–226.
[74] T.X. Italcementi, Millennium Photocatalytic Binders (Technical Report), Italcementi, Italy, 2005.
[75] L. Cassar, Mater. Bull. 29 (2004) 328–331.
[76] G. Bolte, Nanotechnol. Constr. 3 (2009) 55–61.
[77] B. Ruot, A. Plassais, F. Olive, L. Guillot, L. Bonafous, Solar Energy 83 (2009) 1794–1801.
[78] N.S. Allen, M. Edge, J. Verran, J. Stratton, J. Maltby, C. Bygott, Polym. Degrad. Stab. 93 (2008) 1632–1646.
[79] M.M. Hassan, H. Dylla, L.N. Mohammad, T. Rupnow, Constr. Build. Mater. 24 (2010) 1456–1461.
[80] C.J. Churchill, D.K. Panesar, Structure and infrastructure engineering: maintenance management, Life-Cycle Des. Perform. 9 (2013) 983–998.
[81] M. Anpo, P.V. Kamat, Environmentally Benign Photocatalysts: Applications of Titanium Oxide-Based Materials, Springer, Ottawa, Canada, 2010.
[82] N.S. Allen, M. Edge, A. Ortega, G. Sandoval, C.M. Liauw, J. Verran, J. Stratton, R.B. McIntyr, Polym. Degrad. Stab. 85 (2004) 927–946.
[83] T. Yuranova, D. Laub, J. Kiwi Synthesis, Catal. Today 122 (2007) 109–117.
[84] T. Kallio, S. Alajoki, V. Pore, M. Ritala, J. Laine, M. Leskelä, P. Stenius, Colloids Surf. A: Phys. Eng. Asp. 291 (2006) 162–176.
[85] M. Chen, Y. Liu, J. Hazard. Mater. 174 (2010) 375–379.
[86] R. Hela, P. Novosad, J. Valek, J. Prikryl, M. Holak, Proc. Eng. Concr. Concr. Struct. 65 (2013) 20–24.
[87] H. Dylla, M.M. Hassan, M. Schmitt, T. Rupnow, L.N. Mohammad, E. Wright, J. Transp. Res. Board 2240 (2011) 22–29.
[88] R. Cucitore, S. Cangiano, L. Cassar, High durability photocatalytic paving for reducing urban polluting agent, WO Patent 565 (2006).
[89] Y. Murata, H. Tawara, H. Obata, K. Murata, NOX-cleaning paving block, European Patent 786283 (2003).
[90] L. Cassar, P. Carmine, Hydraulic binder and cement compositions containing photocatalyst particles, USA Patent 6409821 (2002).
[91] L. Cassar, C. Pepe, Paving tile comprising an hydraulic binder and photocatalyst particles, European patent 1600430A1 (1997).
[92] A. Folli, I. Pochard, A. Nonat, U.H. Jakobsen, A.M. Shepherd, D.E. Macphee, J. Am. Ceram. Soc. 93 (2010) 3360–3369.
[93] F. Pacheco-Torgal, S. Jalali, Constr. Build. Mater. 25 (2011) 582–590.
[94] N.S. Allen, M. Edge, G. Sandoval, J. Verran, J. Stratton, J. Maltby, Photochem. Photobiol. 81 (2005) 279–290.
[95] L. Frazer, Environ. Health Perspect. 109 (2001) A174–A177.
[96] H. Hamada, K. Komure, R. Takahashi, T. Yamaji, RILEM International Symposium on Environment-Consious Materials and Systems for Sustainable Development, Koriyama, Japan, 2004, pp. 361–366.
[97] D.H. Chen, K. Li, R. Yuan, A. Green, Photocatalytic Coating on Road Pavements/Structures for NO_x Abatement. Annual Project Report, Lamar University, Beaumont, Texas, 2005.
[98] E. Peccati, G.L. Guerrini, Photocatalytic cementitious roads for de-pollution, in: L. Cassar, P. Baglioni (Eds.), Proceedings of Int. RILEM Symposium on Photocatalysis 'Environment and Construction Materials', Florence Italy, 2007, pp. 179–186.
[99] L. Venturini, M. Bacchi, II International Conference Environmentally Friendly Roads ENVIROAD, Warsaw, Poland, 2009.
[100] H. Taoda, Synthesiology 1 (2008) 287–295.
[101] R. Volkamer, U. Platt, K. Wirtz, J. Phys. Chem. A 105 (2001) 7865–7874.
[102] M.G. Vivanco, M. Santiago, A.M. Tarifa, E. Borrás, M. Ródenas, C. García-Diego, M. Sánchez, Atmos. Environ. 45 (2011) 708–715.

[103] B. Zielinska, J. Sagebiel, W. Stockwell, J. McDonald, J. Seagrave, P. Wiesen, K. Wirtz, in: I. Barnes, K. Rudzinski (Eds.), Environmental Simulation Chambers: Application to Atmospheric Chemical Processes, Springer, Netherlands, 2006, pp. 279–284.
[104] S. Hata, Y. Kai, I. Yamanaka, H. Oosaki, K. Hirota, S. Yamazaki, JSAE Rev. 21 (2000) 97–102.
[105] A. Huang, H. Su, J. Environ. Eng. 5 (2011) 477–480.
[106] J. Luo, Y. Xu, W. Zeng, Paint Coat Ind. 41 (2011) 52–55.
[107] M. Mohl, A. Dombovari, E.S. Tuchina, P.O. Petrov, O.A. Bibikova, I. Skovorodkin, A.P. Popov, A.R. Rautio, A. Sarkar, J.P. Mikkola, M. Huuhtanen, S. Vainio, R.L. Keiski, A. Prilepsky, A. Kukovecz, Z. Konya, V.V. Tuchin, J. Mat. Chem. B 2 (2014) 1307–1316.
[108] M. Machida, W.K. Norimoto, T. Kimura, J. Am. Ceram. Soc. 88 (2005) 95–100.
[109] M. Lilja, J. Forsgren, K. Welch, M. Åstrand, H. Engqvist, M. Strømme, Biotechnol. Lett. 34 (2012) 2299–2305.
[110] L. Hochmannova, J. Vytrasova, Prog. Org. Coat. 67 (2010) 1–5.
[111] J. Zhang, S. Li, L. Chen, Y. Pan, S. Yang, IOSR J. Eng. 2 (2012) 50–53.
[112] N. Keller, M.N. Ducamp, D. Robert, V. Keller, Chem. Rev. 113 (2013) 5029–5070.
[113] M.E. Zorn, D.T. Tompkins, W.A. Zeltner, M.A. Anderson, Environ. Sci. Technol. 34 (2000) 5206–5210.
[114] A. Sirisuk, C.G. Hill, M.A. Anderson, Catal. Today 54 (1999) 159–164.
[115] M.E. Zorn, Proceedings of the 13th Annual Wisconsin Space Conference, Wisconsin Space Grant Consortium, Green Bay, WI, 2003.
[116] A. Zapata, I. Oller, E. Bizani, J.A. Sanchez-Perez, M.I. Maldonado, S. Malato, Catal. Today 144 (2009) 94–99.
[117] J. Blanco, S. Malato, P. Fernández, A. Vidal, A. Morales, P. Trincado, J.C. Oliveira, C. Minero, M. Musci, C. Casalle, M. Brunotte, S. Tratzky, N. Dischinger, K.H. Funken, C. Sattler, M. Vincent, M. Collares-Pereira, J.F. Mendes, C.M. Rangel, Solar Energy 67 (2000) 317–330.
[118] E. Watzke, T.h. Kloss, Borosilicatglas mit hoher transmission im UV-Bereich, niedriger Warmedehnung und hoher chemischer Bestandigkeit, Verfahren zu seiner Herstellung und seiner Verwendung, Patent DE4338128C1 (1994).
[119] R.L. Pozzo, J.L. Giombi, M.A. Baltanás, A.E. Cassano, Appl. Catal. B: Environ. 38 (2002) 61–69.
[120] P. Pichat, M. Lu, Photocatalysis and Water Purification: From Fundamentals to Recent Applications, Wiley-VCH, 2013, 2015.
[121] B. Serrano, H. De Lasa, Ind. Eng. Chem. Res. 36 (1997) 4705–4711.
[122] A.H. Geeraerd, V.P. Valdramidis, J.F. Van Impe, Int. J. Food Microbiol. 102 (2005) 95–105.
[123] D.M.A. Alrousan, M.I. Polo-Lopez, P.S.M. Dunlop, P. Fernandez-Ibanez, J.A. Byrne, Appl. Catal. B: Environ. 128 (2012) 126–134.
[124] R.J. Braham, A.T. Harris, Ind. Eng. Chem. Res. 48 (2009) 8890–8905.
[125] S. Malato, J. Blanco, M.I. Maldonado, P. Fernandez, D. Alarcon, M. Collares, J. Farinha, J. Correia, Solar Energy 77 (2004) 513–524.
[126] A. Fernandez-Garcia, E. Zarza, L. Valenzuela, M. Perez, Renew. Sustain. Energy Rev. 14 (2010) 1695–1721.
[127] O. Alfano, D. Bahnemann, A. Cassano, R. Dillert, R. Goslich, Catal. Today 58 (2000) 199–230.
[128] M. Paulescu, E. Paulescu, P. Gravila, V. Badescu, Weather Modeling and Forecasting of PV Systems Operation, Springer Science & Business Media, UK, 2012.
[129] J.V. Anderson, H. Link, M. Bohn, B. Gupta, Solar Energy Mater. 24 (1991) 538–549.
[130] C. Jung, K.H. Funken, J. Ortner, Photochem. Photobiol. Sci. 4 (2005) 409–411.
[131] M. Oelgemoller, C. Jung, J. Ortner, J. Mattay, E. Zimmermann, Green Chem. 7 (2005) 35–38.
[132] N. Monnerie, J. Ortner, J. Solar Energy Eng. 123 (2001) 171–174.
[133] B. Pohlmann, H.D. Scharf, U. Jarolimek, P. Mauermann, Solar Energy 61 (1997) 159–168.
[134] M. Oelgemoller, N. Healy, L. De Oliveira, C. Jung, J. Mattay, Green Chem. 8 (2006) 831–834.
[135] C. Grundmann, Synthesis (1977) 644–645.
[136] G. Oehme, B. Heller, P. Wagler, Energy 22 (1997) 327–336.
[137] J.M. Coronado, F. Fresno, M.D. Hernandez-Alonso, R. Portela, Design of Advanced Photocatalytic Materials for Energy and Environmental Applications, Springer, New York, 2013.
[138] C. Schiel, M. Oelgemoller, J. Ortner, J. Mattay, Green Chem. 3 (2001) 224–228.
[139] M.S. Mehos, C.S. Turchi, Environ. Prog. 12 (1993) 194–199.
[140] R. Dillert, A.E. Cassano, R. Goslich, D.W. Bahnemann, Catal. Today 54 (1999) 267–282.
[141] R.J. Enzweilwer, D.L. Mowery, L.M. Wagg, J.J. Dong, ASME Inter. Solar En. Conf. 26 (13) (1994) 155–161.
[142] G. Zayani, L. Bousselmi, F. Mhenni, A. Ghrabi, Desalination 246 (2009) 344–352.
[143] C. Guillard, J. Disdier, C. Monnet, J. Dussaud, S. Malato, J. Blanco, M.I. Maldonado, J.M. Herrmann, Appl. Catal. B: Environ. 46 (2003) 319–332.
[144] A.J. Feitz, B.H. Boyden, T.D. Waite, Water Res. 34 (2000) 3927–3932.
[145] S.J. Khan, R.H. Reed, M.G. Rasul, BMC Microbiol. 12 (2012) 1–11.
[146] L. Bousseimi, S.U. Geissen, H. Schroeder, Water Sci. Technol. 49 (2004) 331–337.
[147] I.B.S. Will, J.E.F. Moraes, A.C.S. Teixeira, R. Guardani, C.A.O. Nascimento, Sep. Purif. Technol. 34 (2004) 51–57.
[148] C. Heinemann, X. Xing, K.D. Warzecha, P. Ritterskamp, H. Gorner, M. Demuth, Pure Appl. Chem. 70 (1998) 2167–2176.
[149] S. Malato, J. Blanco, C. Richter, D. Curcó, J. Gimenez, Water Sci. Technol. 35 (1997) 157–164.
[150] S.A. Kalogirou, Solar Energy Engineering: Processes Systems, Academic Press, UK, 2014.
[151] W. Gernjak, T. Krutzler, A. Glaser, S. Malato, J. Cáceres, R. Bauer, Chemosphere 50 (2003) 71–78.
[152] J. Garcia-Montano, L. Perez-Estrada, I. Oller, M.I. Maldonado, F. Torrades, J. Peral, Photochem. Photobiol. A: Chem. 195 (2008) 205–214.
[153] I. Oller, W. Gernjak, M.I. Maldonado, L.A. Perez-Estrada, J.A. Sanchez-Perez, S. Malato, J. Hazard. Mater. 138 (2006) 507–517.
[154] S. Malato, J. Blanco, M.I. Maldonado, P. Fernández-Ibanez, W. Gernjak, I. Oller, Chemosphere 58 (2005) 391–398.
[155] P. Fernandez, J. Blanco, C. Sichel, S. Malato, Catal. Today 101 (2005) 345–352.
[156] S. Malato, J. Blanco, M.I. Maldonado, I. Oller, W. Gernjak, L. Pérez-Estrada, J. Hazard. Mater. 146 (2007) 440–446.
[157] V. Sarria, S. Kenfack, O. Guillod, C. Pulgarin, J. Photochem. Photobiol. A: Chem. 159 (2003) 89–99.
[158] T.F.C. Silva, M.E.F. Silva, A.C. Cunha-Queda, A. Fonseca, I. Saraiva, R.A.R. Boaventura, V.J.P. Vilar, Chem. Eng. J. 228 (2013) 850–866.
[159] W. Gernjak, M.I. Maldonado, S. Malato, J. Caceres, T. Krutzler, A. Glaser, R. Bauer, Solar Energy 77 (2004) 567–572.
[160] M. Kositzi, I. Poulios, S. Malato, J. Caceres, A. Campos, Water Res. 38 (2004) 1147–1154.
[161] A. Zapata, I. Oller, C. Sirtori, A. Rodríguez, J.A. Sánchez-Pérez, A. López, M. Mezcua, S. Malato, Chem. Eng. J. 160 (2010) 447–456.
[162] S. Malato, J. Blanco, A. Vidal, P. Fernández, J. Cáceres, P. Trincado, J.C. Oliveira, M. Vincent, Chemosphere 47 (2002) 235–240.
[163] I. Oller, S. Malato, J.A. Sánchez-Pérez, M.I. Maldonado, W. Gernjak, L.A. Pérez-Estrada, A. Muñoz, C. Ramos, C. Pulgarín, Ind. Eng. Chem. Res. 46 (2007) 7467–7475.
[164] J. Blanco, S. Malato, P. Fernández, A. Vidal, A. Morales, P. Trincado, J.C. Oliveira, C. Minero, M. Musci, C. Casalle, M. Brunotte, S. Tratzky, N. Dischinger, K.H. Funken, C. Sattler, M. Vincent, M. Collares-Pereira, J.F. Mendes, C.M. Rangel, Solar Energy 67 (1999) 317–330.
[165] D. Dondi, S. Protti, A. Albini, S. Mañas Carpio, M. Fagnoni, Green Chem. 11 (2009) 1653–1659.
[166] S. Protti, M. Fagnoni, Photochem. Photobiol. Sci. 8 (2009) 1499–1516.
[167] N. Enteria, A. Akbarzadeh, Solar Energy Sciences and Engineering Applications, CRC Press, UK, 2013.
[168] H. Brown, A.W. Hewett, R. Gee, K. May, Energy Eng. 94 (1997) 33–44.
[169] J.I. Ajona, A. Vidal, Solar Energy 68 (2000) 109–120.
[170] J.R. Bolton, K.G. Bircher, W. Tumas, C.A. Tolman, Pure Appl. Chem. 73 (2001) 627–637.
[171] E.R. Bandala, M.A. Pelaez, A.J. Garcıa-Lopez, M.J. Salgado, G. Moeller, Chem. Eng. Process. 47 (2008) 169–176.
[172] J.A. Martinez-Lozano, F. Tena, M.P. Utrillas, Int. J. Climatol. 19 (1999) 903–911.
[173] A. Podstawczynska, Int. J. Climatol. 30 (2010) 1–10.
[174] R. Bauer, G. Waldner, H. Fallmann, S. Hager, M. Klare, T. Krutzler, S. Malato, P. Maletzky, Catal. Today 53 (1999) 131–144.
[175] G. Mailhot, M. Sarakha, B. Lavedrine, J. Caceres, S. Malato, Chemosphere 49 (2002) 525–532.
[176] E.R. Bandala, C. Estrada, J. Solar Energy Eng. 129 (2007) 22–26.
[177] R. Marotta, D. Spasiano, I. Di Somma, R. Andreozzi, V. Caprio, Chem. Eng. J. 209 (2012) 69–78.
[178] S. Protti, D. Ravelli, M. Fagnoni, A. Albini, Chem. Commun. 47 (2009) 7351–7353.
[179] T. Caronna, C. Gambarotti, L. Palmisano, C. Punta, F. Recupero, J. Photochem. Photobiol. A: Chem. 171 (2005) 237–242.
[180] R.A. Doohan, N.W.A. Geraghty, Green Chem. 7 (2005) 91–96.
[181] L. Cermenati, C. Richter, A. Albini, Chem. Commun. 7 (1998) 805–806.
[182] J. Benites, D. Rios, P. Díaz, J.A. Valderrama, Tetrahedron Lett. 52 (2011) 609–611.

[183] T. Caronna, C. Gambarotti, L. Palmisano, C. Punta, M. Pierini, F. Recupero, J. Photochem. Photobiol. A: Chem. 189 (2007) 322–328.
[184] M.A. McGuire, L.S. Hegedus, J. Am. Chem. Soc. 104 (1982) 5538–5540.
[185] M.A. Ischay, M.E. Anzovino, J. Du, T.P. Yoon, J. Am. Chem. Soc. 130 (2008) 12886–12887.
[186] A.G. Griesbeck, T.T. El-Idreesy, A. Bartoschek, Appl. Chem. 77 (2005) 1059–1074.
[187] N. Hoffmann, Chem. Rev. 108 (2008) 1052–1103.
[188] S. Marinkovic, C. Brule, N. Hoffmann, E. Prost, J.M. Nuzillard, V.J. Bulach, J. Org. Chem. 69 (2004) 1646–1651.
[189] K. Takami, J. Yamamoto, K. Komeyama, T. Kawabata, K. Takeira, Bull. Chem. Soc. Jpn. 77 (2004) 2251–2255.
[190] A. Itoh, S. Hashimoto, K. Kuwabara, T. Kodama, Y. Masaki, Green Chem. 7 (2005) 830–832.
[191] E. Haggiage, E.E. Coyle, K. Joyce, M. Oelgemoller, Green Chem. 11 (2009) 318–321.
[192] D.T. Santos, J.Q. Albarelli, K. Joyce, M. Oelgemoller, J. Chem. Technol. Biotechnol. 84 (2009) 1026–1030.
[193] K. Sivaranjani, C.S. Gopinath, J. Mater. Chem. 21 (2011) 2639–2647.
[194] K. Wiesner, J.G. McCluskey, J.K. Chang, V. Smula, Can. J. Chem. 49 (1971) 1092–1098.
[195] Y.P. Zhao, R.O. Campbell, R.S.H. Liu, Green Chem. 10 (2008) 1038–1042.
[196] Y. Zhao, L. Yang, R.S.H. Liu, Green Chem. 11 (2009) 837–842.
[197] T. Caronna, C. Gambarotti, A. Mele, M. Pierini, C. Punta, F. Recupero, Res. Chem. Intermed. 33 (2007) 311–317.
[198] D. Elad, J. Rokach, J. Chem. Soc. 1 (1965) 800–802.
[199] D. Elad, J. Rokach, J. Org. Chem. 30 (1965) 3361–3364.
[200] Y. Pan, C.W. Kee, L. Chen, C.H. Tan, Green Chem. 13 (2011) 2682–2685.
[201] A. García-Ripoll, A. Arques, R. Vicente, A. Domenech, A.M. Amat, Solar Energy Eng. 130 (2008) 41011/1–41011/5.
[202] N. Miranda-García, S. Suárez, B. Sánchez, J.M. Coronado, S. Malato, M.I. Maldonado, Appl. Catal. B: Environ. 103 (2011) 294–301.
[203] J.M. Herrmann, J. Disdier, P. Pichat, S. Malato, J. Blanco, Appl. Catal. B: Environ. 17 (1998) 15–23.
[204] J.H.O.S. Pereira, V.J.P. Vilar, M.T. Borges, O. Gonzalez, S. Esplugas, R.A.R. Boaventura, Solar Energy 85 (2011) 2732–2740.
[205] E. Remoundaki, R. Vidali, P. Kousi, A. Hatzikioseyian, M. Tsezo, Desalination 248 (2009) 843–851.
[206] F. Correia, V. Goetz, G. Plantard, D. Sacco, J. Solar Energy Eng. 133 (2011) 31002/1–31002/5.
[207] S. Malato, J. Caceres, A. Aguera, M. Mezcua, D. Hernando, J. Vial, A.R. Fernandez-Anda, Environ. Sci. Technol. 35 (2001) 4359–4366.
[208] R. Krutzler, H. Fallmann, P. Maletzky, R. Bauer, S. Malato, J. Blanco, Catal. Today 54 (1999) 321–327.
[209] M.S. Lucas, R. Mosteo, M.I. Maldonado, S. Malato, J.A. Peres, J. Agric. Food Chem. 57 (2009) 11242–11248.
[210] E. Ubomba-Jaswa, C. Navntoft, I. Polo-López, P. Fernández-Ibáñez, K.G. McGuigan, Photochem. Photobiol. Sci. 8 (2009) 587–595.
[211] C. Sichel, J.C. Tello, M. De Cara, P. Fernández-Ibáñez, Catal. Today 129 (2007) 152–160.
[212] M.I. Polo-López, P. Fernández-Ibáñez, E. Ubomba-Jaswa, C. Navntoft, I. Garcia-Fernandez, P.S.M. Dunlop, M. Schmidt, J.A. Byrne, K.G. McGuigan, J. Hazard. Mater. 196 (2011) 16–21.
[213] E. Ubomba-Jaswa, P. Fernández-Ibáñez, C. Navntoft, M.I. Polo-López, K.G. McGuigan, J. Chem. Technol. Biotech. 85 (2010) 1028–1037.
[214] C.S.D. Rodrigues, L.M. Madeira, R.A.R. Boaventura, Ind. Eng. Chem. Res. 52 (2013) 13313–13324.
[215] D. Weinstock, J. Appelbaum, J. Solar Energy Eng. 126 (2004) 898–905.
[216] P.R. Gogate, A.B. Pandit, AIChE J. 50 (2004) 1051–1079.
[217] A.M.T. Silva, E. Nouli, N.P. Xekoukoulotakis, D. Mantzavinos, Appl. Catal. B: Environ. 73 (2007) 11–22.
[218] V.K. Pareek, A.A. Adesina, in: H.S. Nalwa (Ed.), Handbook of Photochemistry and Photobiology, Vol. 1, American Scientific Publishers, Stevenson Ranch, 2003, pp. 345–412.
[219] A.E. Cassano, O.M. Alfano, Catal. Today 58 (2000) 167–197.
[220] R.L. Romero, O.M. Alfano, A.E. Cassano, Ind. Eng. Chem. Res. 36 (1997) 3094–3109.
[221] M.I. Cabrera, O.M. Alfano, A.E. Cassano, J. Phys. Chem. 100 (1996) 20043–20050.
[222] P. Fernandez-Ibanez, S. Malato, F.J. De Las Nieves, Catal. Today 54 (1999) 195–204.
[223] C. Guillard, J. Disdier, J.M. Herrmann, C. Lehaut, T. Chopin, S. Malato, J. Blanco, Catal. Today 54 (1999) 217–228.
[224] J. Jimenez, D. Curco, M.A. Queral, Catal. Today 54 (1999) 229–244.
[225] G. Camera-Roda, F. Santarelli, Catal. Today 129 (2007) 161–168.
[226] D. Chen, F. Li, A.K. Ray, AICHE 46 (2000) 1034–1045.
[227] J. Ryu, W. Cho, Environ. Sci. Technol. 42 (2008) 294–300.
[228] A.G. Agrios, P. Pichat, J. Photochem. Photobiol. A 180 (2006) 130–135.
[229] D. Hufschmidt, D. Bahnemann, J.J. Testa, C.A. Emilio, M.I. Litter, J. Photochem. Photobiol. A 148 (2002) 223–231.
[230] H. Fallmann, T. Krutzler, R. Bauer, S. Malato, J. Blanco, Catal. Today 54 (1999) 309–319.
[231] C.S. Zalazar, C.A. Martin, A.E. Cassano, Chem. Eng. Sci. 60 (2005) 4311–4322.
[232] D.D. Dionysiou, A.A. Burbano, M.T. Suidan, Environ. Sci. Technol. 36 (2002) 3834–3843.
[233] A. Piscopo, D. Robert, J.V. Weber, Appl. Catal. B: Environ. 35 (2001) 117–124.
[234] K.H. Wang, Y.H. Hsieh, M.Y. Chou, C.Y. Chang, Appl. Catal. B: Environ. 21 (1999) 1–8.
[235] I.K. Konstantinou, T.A. Albanis, Appl. Catal. B: Environ. 49 (2004) 1–14.
[236] M. Kosmulski, J. Colloids Interface Sci. 353 (2011) 1–15.
[237] G.A. Parks, Chem. Rev. 65 (1965) 177–198.
[238] Y. Zhang, Y. Chen, P. Westerhoff, K. Hristovski, J.C. Crittenden, Water Res. 42 (2008) 2204–2212.
[239] M.L. Machesky, D.J. Wesolowski, D.A. Palmer, K. Ichiro-Hayashi, J. Colloids Interface Sci. 200 (1998) 298–309.
[240] K. Nagaveni, M.S. Hegde, N. Ravishankar, G.N. Subbanna, G. Madras, Langmuir 20 (2004) 2900–2907.
[241] T. Hathway, W.S. Jenks, J. Photochem. Photobiol. A: Chem. 200 (2008) 216–224.
[242] I. Christl, R. Kretzschmar, Geochim. Cosmochim. Acta 63 (1999) 2929–2938.
[243] C. Tso, C. Zhung, Y. Shih, Y.M. Tseng, S. Wu, R. Doong, Water Sci. Technol. 61 (2010) 127–133.
[244] V. Augugliaro, C. Baiocchi, A.B. Prevot, E. García-López, V. Loddo, S. Malato, G. Marcí, L. Palmisano, M. Pazzi, E. Pramauro, Chemosphere 49 (2002) 1223–1230.
[245] H. Lachheb, E. Puzenat, A. Houas, M. Ksibi, E. Elaloui, C. Guillard, J.M. Herrmann, Appl. Catal. B: Environ. 39 (2002) 75–90.
[246] Y. Xu, C.H. Langford, J. Photochem. Photobiol. A: Chem. 133 (2000) 67–71.
[247] A.A. Bilgin, J. Silverstein, M. Hernandez, Environ. Sci. Technol. 39 (2005) 7826–7832.
[248] M.S. Lucas, J.A. Peres, Dyes Pigm. 71 (2006) 236–244.
[249] M.I. Badawy, M.Y. Ghaly, T.A. Gad-AllaH, Desalination 194 (2006) 166–175.
[250] B.G. Kwon, D.S. Lee, N. Kang, J. Yoon, Water Res. 33 (1999) 2110–2118.
[251] L. Prieto-Rodríguez, D. Spasiano, I. Oller, I. Fernández-Calderero, A. Agüera, S. Malato, Catal. Today 209 (2013) 188–194.
[252] H. Krýsová, J. Jirkovský, J. Krýsa, G. Mailhot, M. Bolte, Appl. Catal. B: Environ. 40 (2003) 1–12.
[253] M. Kositzi, I. Poulios, K. Samara, E. Tsatsaroni, E. Darakas, J. Hazard. Mater. 146 (2007) 680–685.
[254] H. Al-Ekabi, P. Mayo, J. Phys. Chem. 89 (1985) 5815–5821.
[255] S. Mozia, M. Tomaszewska, A.W. Morawski, Desalination 185 (2005) 449–456.
[256] J.M. Herrmann, Top. Catal. 34 (2005) 49–65.
[257] G. Ciamician, Science 36 (1912) 385–394.